Time series analysis of tegument ultrastructure of in vitro transformed miracidium to mother sporocyst of the human parasite Schistosoma mansoni

Pierre Poteaux, Benjamin Gourbal, David Duval

Time series analysis of tegument ultrastructure of *in vitro* transformed miracidium to mother sporocyst of the human parasite *Schistosoma mansoni*

Pierre Poteaux*, Benjamin Gourbal, David Duval

IHPE, CNRS, IFREMER, Univ Montpellier, Univ Perpignan Via Domitia, Perpignan, France

ABSTRACT

The transformation of *Schistosoma mansoni* miracidia into mother sporocysts is induced, either *in vivo* by the penetration of the free-living larval stage, the miracidium, in the snail *Biomphalaria glabrata* or *in vitro* following the incubation of the miracidium in Chernin's Balanced Salt Solution (CBSS) or Bge (*B. glabrata* embryonic cell line) culture medium. The *in vitro* development of *S. mansoni* miracidium into mother sporocyst was monitored by Scanning Electron Microscopy (SEM) from 2.5 h to 120 h in CBSS. The transformation starts when the miracidium ciliate plates detach due to the proliferation of the intercellular ridge associated with the degeneration of mid-body papillae of the miracidium. The loss of ciliated plates causes the appearing of scars, filled across time by the proliferation of a new tegument originating from the interplate ridge. This new tegument covers the entire body of the metamorphosing parasite and differentiates over time, allowing some exchanges (uptakes or secretion/excretion) between the parasite and its host. In contrast to the well-described development of adult and free-living larval stages of *S. mansoni* using SEM, the developmental transformation of intramolluscan stages, especially tegumental changes in the mother sporocyst, has been sparcely documented at the ultrastructural level. In addition, taking into account the latest literature on miracidium electron microscopy and the advances in SEM technologies over the last thirty years, the present study gathers three main objectives: (i) Fill the gap of tegument scanning electron micrographs of *in vitro* transforming sporocysts; (ii) Update the current bibliographic miracidia and sporocysts image bank due to rapid evolution of SEM technology; (iii) Understand and describe the critical steps and duration of the *in vitro* miracidium-to-sporocyst transformation process to assist in understanding the interaction between the larval surface and snail immune factors.

KEYWORDS

Schistosoma mansoni – Ultrastructure – Mother sporocyst – Miracidium – Scanning Electron Microscopy

1. Introduction

The trematode parasite *Schistosoma mansoni* has a complex life cycle, involving freshwater snails as intermediate hosts and mammals as definitive hosts, each host type being infested by a particular free-living infective stage of the parasite. Those two stages, the ciliated larva miracidium and the forked tailed (furco)cercaria exhibit different specificity for their hosts. The miracidium of *S. mansoni* parasitizes a restricted intermediate host spectrum consisting of few snail species (Campos et al., 2002; Galinier et al., 2017; Fuss et al., 2020) while cercariae exhibit a wide host range, being able to infest several mammal genera and species (Catalano et al., 2020; Kebede et al., 2020). Those very different living conditions imply specific contexts of molecular interactions of these life stages with their hosts and thus necessitate specific adaptations to establish and to maintain within their host, especially for the tegument structure (Meuleman et al., 1978; Lodes and Yoshino, 1989; Dalton et al., 2004; Hambrook et al., 2018). Using electron microscopy, the ultrastructure of *Schistosoma* tegument has been well-documented for the free-living stages of the parasite. For example, miracidia tegument structure has been described in depth under different aspects, considering the global shape of the miracidium larva (Sakamoto and Ishii, 1978; Pan, 1980), the description of the ciliated plates (Hansen and Perez-Mendez, 1972; Koie and Frandsen, 1976), of the terebratorium (LoVerde, 1975; Eklu-Natey et al., 1985; Kruger and Hamilton-Attwell, 1988) or of other sensing papillae (Samuelson and Caulfield, 1985; Daniel et al., 1992). Cercariae tegumental structure has been also well described (Sakamoto and Ishii, 1978; Pereira et al., 2013). In addition, the vertebrate stages of the parasite (*i.e.* schistosomula and adult stages) have been thoroughly described, especially following biomedical stress exposures, for examples, to the anti-schistosomal drug praziquantel or other experimental treatment compounds, to oxidative stressors or ethanol (Kamel and Bayaumy, 2017; Amara et al., 2018; Araújo et al., 2019, 2020; Brandao-Bezerra et al., 2019˜ ; Zoghroban et al., 2019). Concerning the development of miracidia to mature sporocysts, the ultrastructural changes of surface tegument remained seldom studied (Samuelson and Caulfield, 1985; Daniel et al., 1992; Dinguirard et al., 2018). This lack of data may be explained by limitations in maintaining miracidia under sterile culture conditions and difficulties encountered in sample preparation. Despite these limitations, however, responses of *in vitro* transformed miracidia to snail hemolymph or recombinant proteins have been reported (Bender et al., 2002; Portet et al., 2017; Li et al., 2020; Hambrook and Hanington, 2021). Thus, it seems useful to have access to reference images of transforming *S. mansoni* mother sporocysts through time at least to estimate the tegument characteristics of a fully transformed sporocyst *in vitro*. Also, this will allow the use of these reference data for conducting functional studies on sporocyst tegument damages following exposure to cytotoxic or cytolytic treatments.

This work aims to fill this gap and put forward micrographs of transforming sporocysts to highlight the surface tegument ultrastructural changes occurring during this early intra-molluscal life stage. All the micrographs produced will be shared with the international community to update the bibliographical image bank with those more recent scanning electron microscopy images (access: 10.5281/zenodo. 7468209).

2. Methods

2.1. Ethics statement

Our laboratory holds permit # A66040 for experiments on animals from both the French Ministry of Agriculture and Fisheries, and the French Ministry of National Education, Research, and Technology. The housing, breeding and animal care of the utilized animals followed the ethical requirements of our country. The researchers also possess an official certificate for animal experimentation from both French ministries (Decree # 87–848, October 19, 1987). Animal experimentation followed the guidelines of the French CNRS. The different protocols used in this study had been approved by the French veterinary agency from the DDPP Languedoc–Roussillon (Direction Departementale de Protec´ tion des Populations), Montpellier, France (authorization # 007083) and the Ethic committee CEEA-LR (# C66-136-01).

2.2. Parasite recovery and in-vitro culture conditions

Golden hamsters (*Mesocricetus auratus*) were infested with 2000 cercariae of *S. mansoni* NMRI strain. Seven weeks post-infection, hamsters' livers were recovered in saline solution (150 mM NaCl), grinded and eggs were filtered using sieves. Eggs were hatched in sterile fresh water. Miracidia were concentrated by sedimentation on ice before being placed in culture buffer. Primary sporocysts were obtained in Chernin's Balanced Salt Solution (CBSS) trehalose depleted (Chernin, 1963) supplemented with antibiotics (0.1 mg mL^{-1} streptomycin, 0.25 µg mL^{-1} Amphotericin B and 100 U mL^{-1} penicillin) and maintained at 27 °C under normoxic condition for several hours depending on the transformation time chosen (2.5, 4, 6, 12, 24, 48, 97 or 120 h of transformation). *2.3. Parasite fixation*

Miracidia were fixed with 3% glutaraldehyde (glutaraldehyde 50% Aqueous Solution, Electron Microscopy Sciences) in 100 mM sodium cacodylate (0.2 M Sodium cacodylate Solution Electron Microscopy Sciences, pH 7.4) diluted in sterile water. Sporocysts were fixed for each time point using the same procedure except that water was replaced by CBSS trehalose depleted (Chernin, 1963). Fixation occurred for at least 24 h at 4 °C. Then, fixed samples were washed for 15 min two times in 100 mM sodium cacodylate diluted in Phosphate Buffered Saline and placed in 70% ethanol until used.

2.4. Supercritical drying

Samples were exposed to 3 ethanol bathes, 10 min each (85%, 95% and 100%). Samples in 100% ethanol were put in 30 µm diameter microporous specimen capsules (Electron Microscopy Sciences) for drying. Capsules were then placed into a Balzers Union Supercritical drying system in which ethanol is slowly replaced with liquid CO_2 (Pressure reaches around 50 Bar, temperature kept under 10 °C). After ethanol is totally replaced, the chamber is heated up to 40 °C (Pressure is around 73 Bar). The chamber is finally isothermally depressurized and dry samples are deposited on carbon adhesive for metal coating of specimens.

2.5. Sputter coating of specimens and visualization

Metal coating of specimens is performed in an SC 500 Emscope metal coating system by Ar plasma. Samples are coated with Au/Pd for 2 min and 20 s (7.5 mA). Visualization was performed with a Hitachi Scanning Electron Microscope, mounted with a S-4500 tungsten cold source Field Emission Gun (Tokyo, Japan). Acceleration voltage was set at 5 kV. Everhardt Thornley chamber detector was used. For some of the pictures, in-lens detector was used.

3. Results

3.1. General morphological aspect of miracidium

Miracidia were about 110 µm long for about 27 µm width with a median narrowing area (about 20 µm) (Fig. 1). One can notice the great number of cilia along the larva exhibiting a different organization between the apex and the body (Figs. 1–4). Those apex "cilia" are specifically localized on an area that stretches up to 11 µm from the terebratorium (when uncontracted). Those structures look curved backwards and barb-shaped, probably helping the organism to fix and penetrate in host tissues. Two lateral apical smooth papillae were observed through the cilia, measuring around 1.8 µm in diameter (Figs. 1–4).

3.1.1. Terebratorium

In the species *S. mansoni*, the apical papilla, called terebratorium, exhibits specific anastomosing folds exposing uni- and multiciliated receptors (Figs. 5–8) (Eklu-Natey et al., 1985). Terebratorium measures approximately 7 µm in diameter and 3.5 to 5 µm in length and is covered by several ciliated nerve endings, constituting uniciliated receptors (Figs. 4, 5, 6 and 8) and some multiciliated receptors (Figs. 5 and 7). Four uniciliated receptors were visible on both lateral sides of the terebratorium framing the multiciliated receptors, which are usually grouped by pairs. On the presented terebratorium (Fig. 5), three multiciliated receptor mouths seem to be visible on one side of the terebratorium. Two uniciliated receptors were noticed on the top of the terebratoria. Often a globular structure seemed to leave the base of the terebratorium, suggesting the presence of lateral gland apertures (LG) (Figs. 4 and 5).

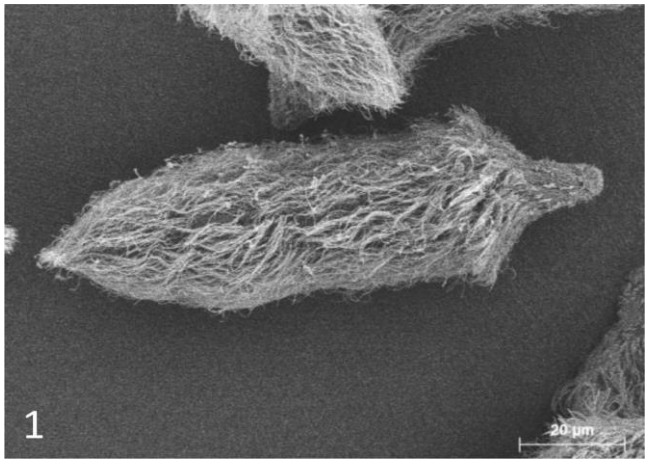

Fig. 1. Scanning electron micrographs of miracidium larvae of *S. mansoni*. 1 Miracidium of *S. mansoni* × 1000.

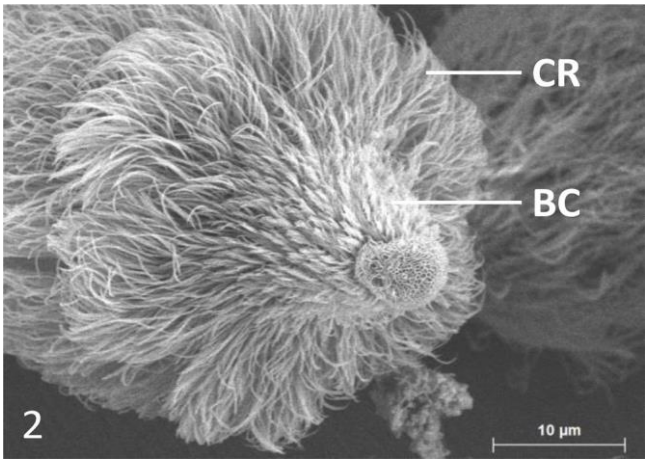

Fig. 2. Front view of the apex of a miracidium × 2500 showing the transition between barb- shaped cilia (BC) and locomotor cilia arranged in a collar in the first third of the animal (CR).

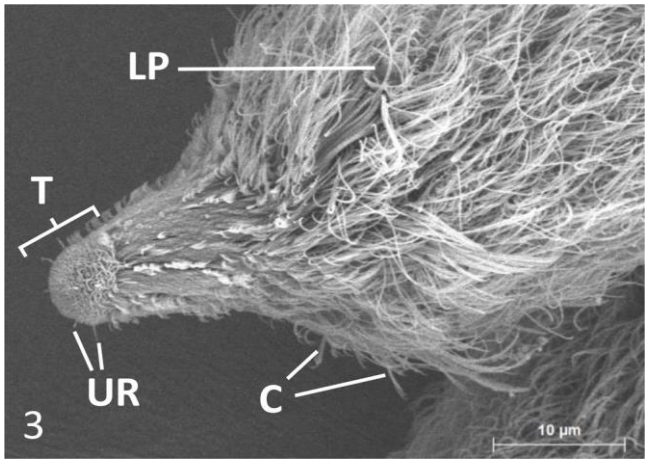

Fig. 3. Lateral view of the apex of a miracidium × 2500 showing one of the Two lateral papilla (LP), the relative size of the apical papilla called Terebratorium (T) and ciliated nerve ending i. e. uniciliated receptors on the tere-bratorium (UR).

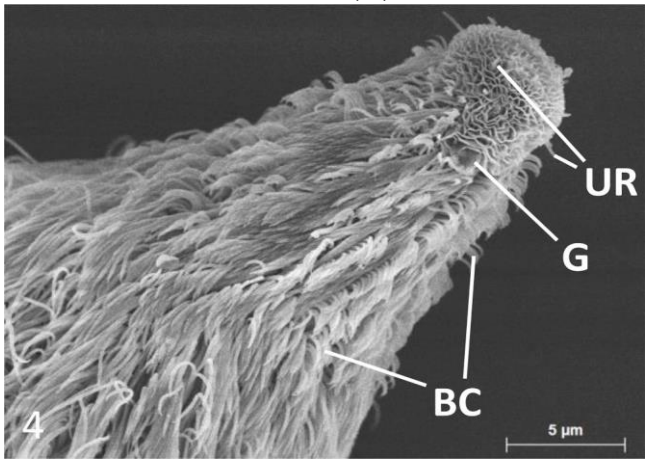

Fig. 4. Magnification of the apex of a miracidium × 4500. Globular structure (G) can sometimes be noticed in the basal area of the terebratorium, possibly linked to lateral gland secretions. Short barb-shaped cilia are well noticeable(BC) as well as uniciliated receptors (UR) of the terebratorium

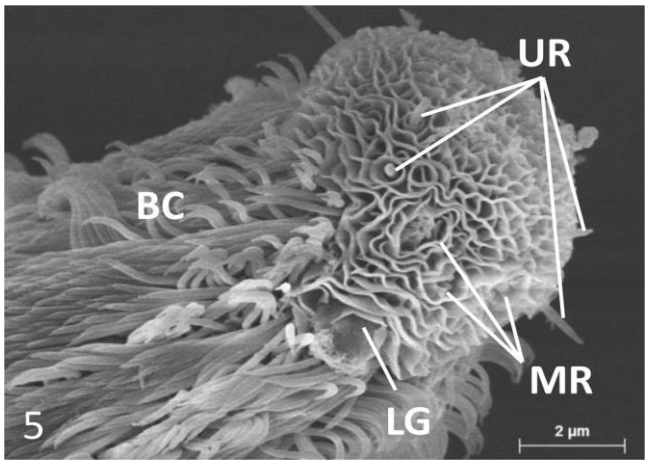

Fig. 5. Scanning electron micrographs of the apical papilla of miracidium larvae of *S. mansoni*. 5 Terebratorium of a miracidium × 10,000 exhibiting multiciliated receptors or papillae (MR) and lateral gland opening (LG), no barb-shaped cilia (BC) were noticeable on the terebratorium.

3.1.2. Tegument

The tegument is constituted of ciliated plates separated by an unciliated syncytial interplate tegument (also called intercellular ridge) (Figs. 9–11). Ciliated plates and syncytial tegument exhibit rugous aspect, this rugosity is denser on the ciliated plates, comparing to the syncytial tegument. Cilia were 0.14 µm thick in diameter. Roughness granules were about 0.1 µm of diameter (Fig. 11). We were able to visualize excretory pores in the last posterior third, the opening is 1 µm (Figs. 9, 10 and 12). Our observations were consistent with the study of Koie and Frandsen (1976).

3.2. Miracidium to sporocyst transformation

3.2.1. Time point 2.5 h

3.2.1.1. General. Interplate tegument started to be apparent less than 3 h after the beginning of the incubation and miracidia were mostly contracted (approximately 63 µm in length), especially at the apex, helping them to free the ciliated plates. After 2.5 h of incubation in CBSS, miracidia started to stop swimming and sediment on the culture plate. About half of the larvae were still uncontracted swimming miracidia (Fig. 13). No detached ciliated plates were visible in the culture medium at that point (Fig. 13).

3.2.1.2. Apex. The terebratorium was intact and the apex contracted, depending on the individuals (Figs. 14 and 15). No specific morphological changes were noticed at this step in the apical region.

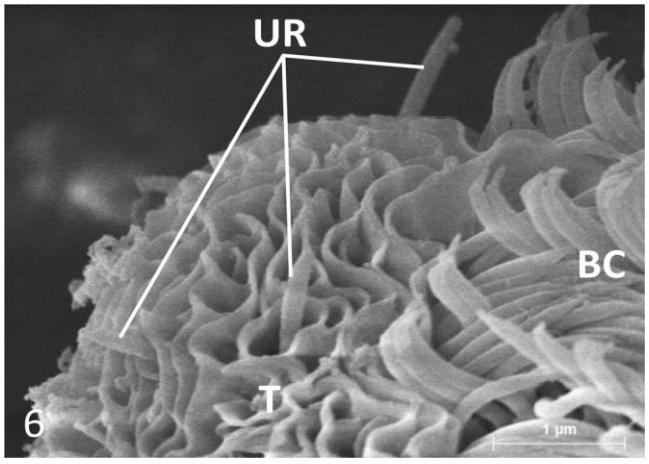

Fig. 6. Terebratorium (details) × 25,000 showing the transition between the apical papilla (T) and barb-shaped cilia (BC).

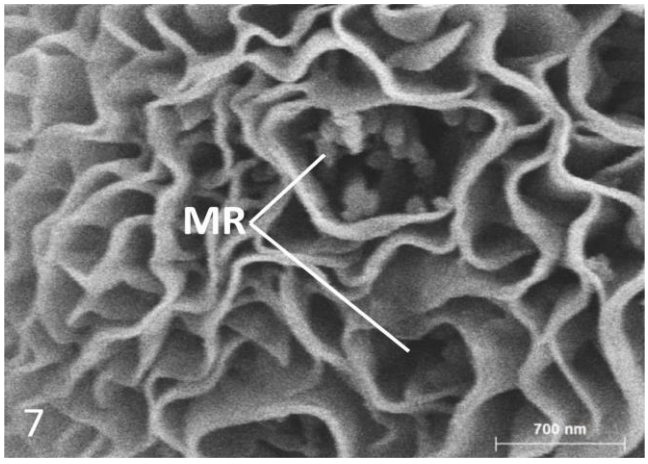

Fig. 7. Focus on multiciliated receptor or multiciliated papillae (MR) × 35,000.

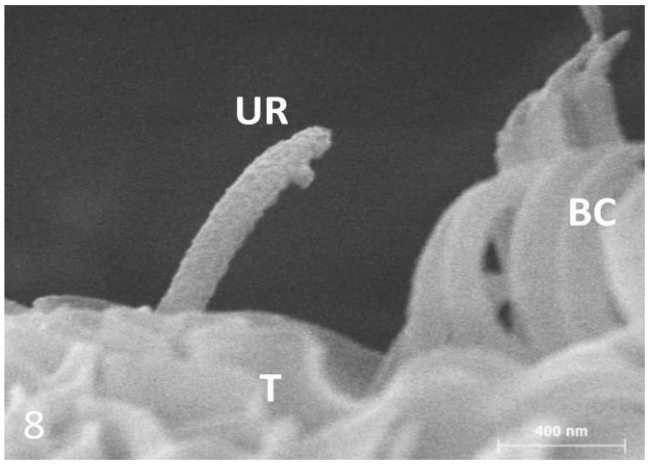

Fig. 8. Magnification of a ciliate nerve ending × 60,000 showing the typical shape and rugous aspect of the uniciliated receptors (UR) on a terebratorium (T) compared to the other barb-shaped cilia (BC).

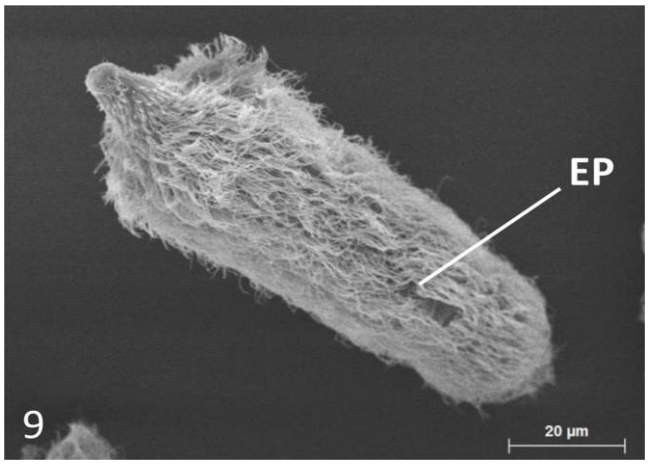

Fig. 9. Scanning electron micrographs of miracidium. 9 Miracidium of *S. mansoni* × 1100 on which an excretory pore is visible in the last third of the larva.

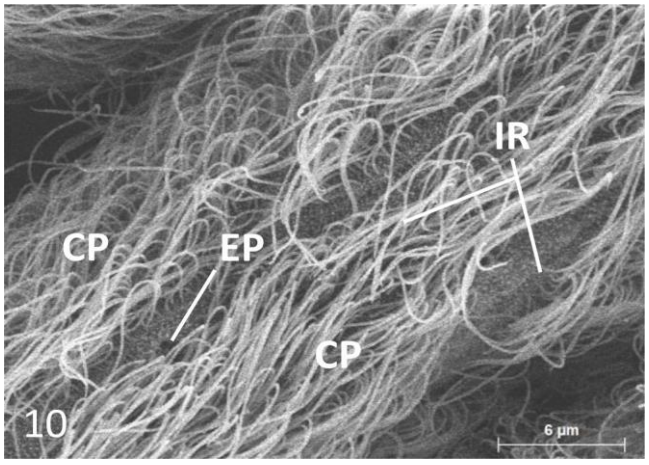

Fig. 10. Miracidium surface × 4000 showing ciliated plates (CP), inter--cellular ridges (IR) and an excretory pore (EP).

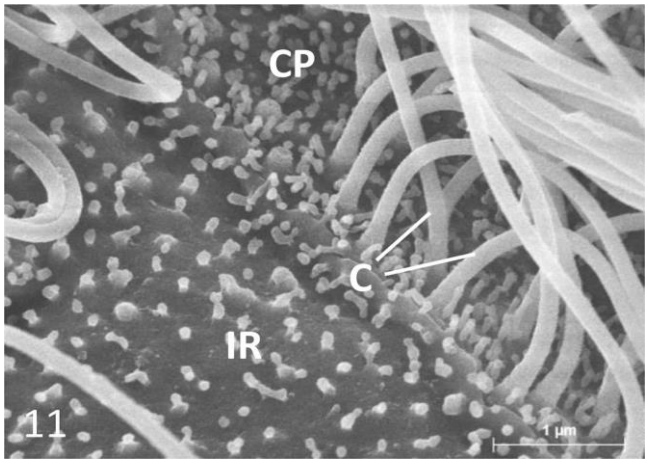

Fig. 11. Magnification of the edge of a ciliated plate × 25,000 showing the tegument granularity differences between the intercellular ridge (IR) and a ciliated plate (CP) wearing the locomotor cilia (C).

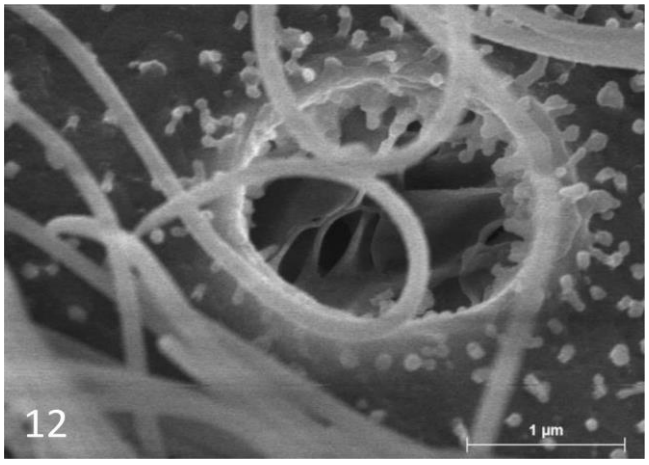

Fig. 12. Magnification of an excretory pore × 30,000.

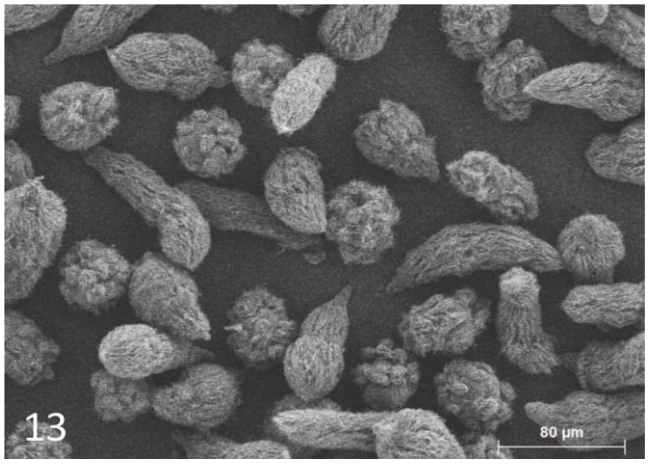

Fig. 13. Scanning electron micrographs of 2.5 h transforming miracidia. 13 Transforming miracidia of *S. mansoni* (2.5 h) × 300.

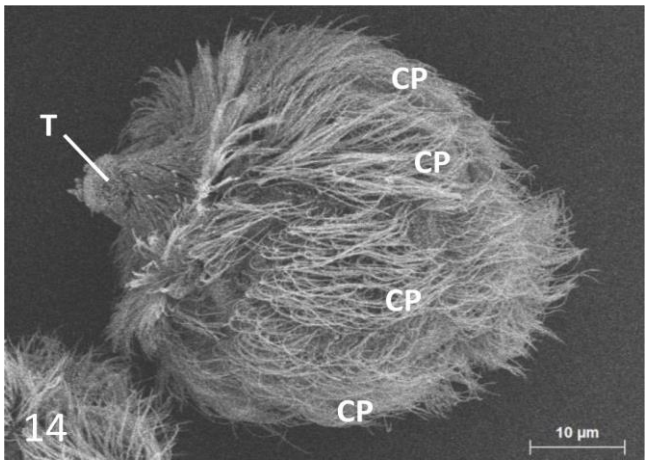

Fig. 14. Transforming miracidium of *S. mansoni* (2.5 h) × 1800, note the proliferation of the interplate ridge and the characteristic ciliated plate (CP) number and arrangement of the species *mansoni*. The apex topped by the terebratorium (T) is contracted.

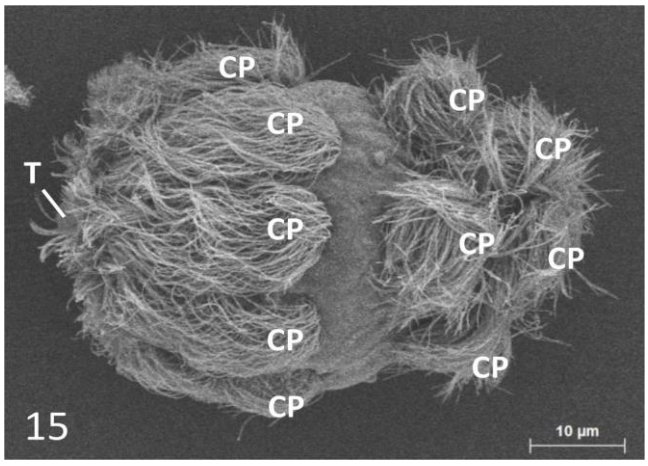

Fig. 15. Transforming miracidium of *S. mansoni* (2.5 h) × 1800, note the proliferation of the interplate ridge and the characteristic ciliated plate (CP) number and arrangement of the species *mansoni*.
The apex topped by the terebratorium (T) is contracted.

3.2.1.3. Tegument. Depending on the individuals, the proliferative tegument was visible between the ciliated plates. This tegument seems smoother than the ciliated plates surface. Ciliated plates separation due to intercellular (or interplate) ridges proliferation was visible and their expansion was different depending on the individuals considered (Figs. 14–17). Multiciliated receptors were noticeable, emerging from this newly appearing tegument, those receptors are found on miracidia between the second and third tier of the larva (Fig. 17) (Eklu-Natey et al., 1985; Samuelson and Caulfield, 1985).

3.2.2. Time point 4 h

3.2.2.1. General. Miracidia lose nearly all their ciliated plates, showing scars and lateral papillae. Remnant plates persist in the apical region. Larvae remained contracted as at 2.5 h time point (Fig. 18).

3.2.2.2. Apex. Most miracidia were still showing plates detaching from the apical region, suggesting a particular shedding order of the plates starting from the posterior part of the larva (Figs. 19 and 20), this is consistent with previous observations (Samuelson and Caulfield, 1985; Daniel et al., 1992). Depending on the individuals, some miracidia lost nearly all their ciliated plates while some kept their first third plates, some of them lost their terebratorium while some others not (Figs. 19–21).

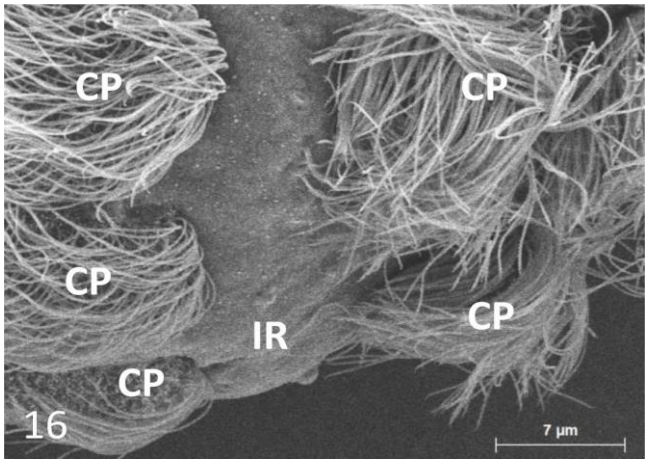

Fig. 16. Scanning electron micrographs of 2.5 h transforming miracidia. 16 Details of the interplate tegument showing an enlargement of the intercellular ridge (IR) between the ciliated plates (CP) × 3500.

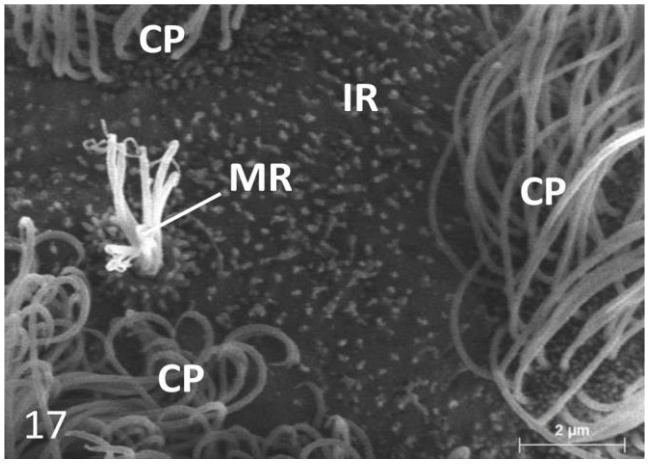

Fig. 17. Focus on a multiciliated receptor (MR) emerging from the interplate ridge × 10,000.

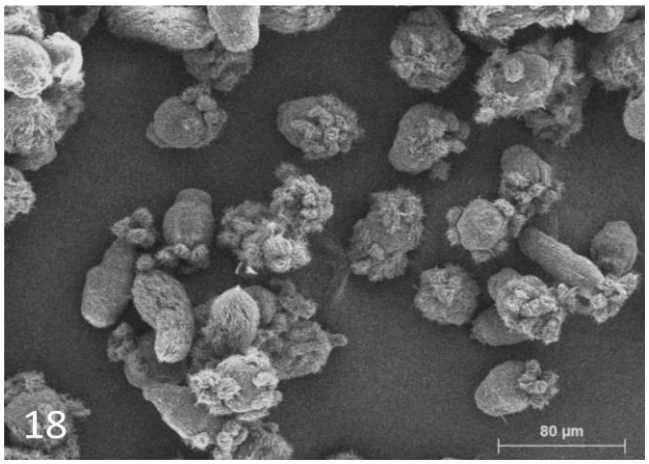

Fig. 18. Scanning electron micrographs of 4 h transforming miracidia. 18 Transforming miracidia of *S. mansoni* (4 h) × 300.

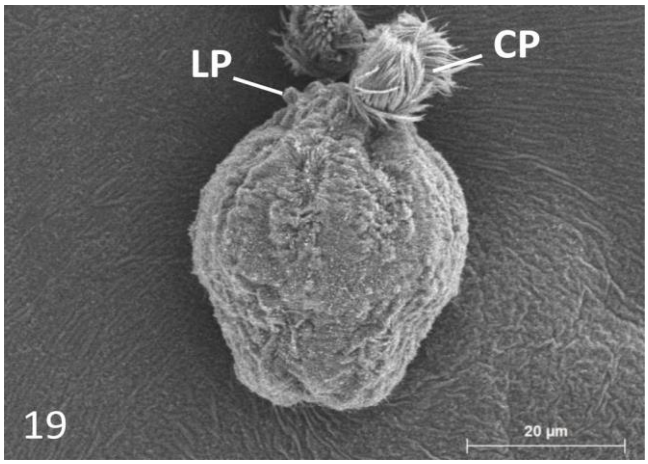

Fig. 19. Focus on single transforming individual × 1500, lateral papillae (LP) and remnant circular ciliated plates (CP) can be noticed.

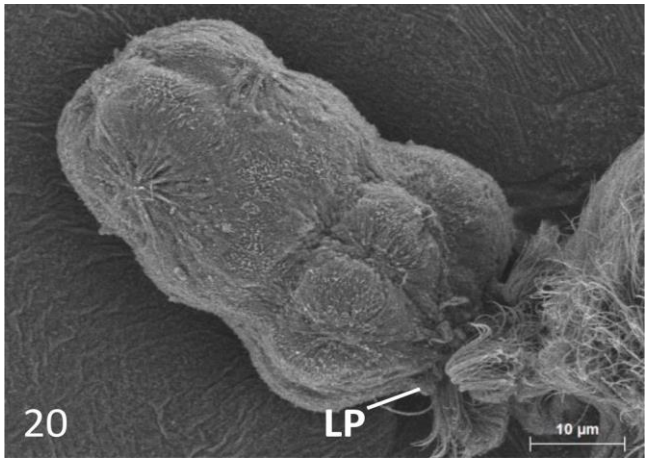

Fig. 20. Focus on single transforming individual × 1500, lateral papillae (LP) and remnant circular ciliated plates (CP) can be noticed.

3.2.2.3. Tegument. Several scars are visible at the location of the previously detached ciliated plates, forming trenches in-between the new proliferative tegument in the apical first half of the miracidium body (Figs. 19, 20 and 22–24) and forming star-like scars in the bottom part of the transforming miracidia (Figs. 20, 23 and 25). Multiciliated receptors previously noticed on the body of the miracidium are now degenerating (Fig. 23). In the apical region, the loss of terebratorium seems to induce the appearing of remnant shreds on the tegument close to apex (Fig. 24). We can notice the proliferative tegument exhibiting rugous aspect in- between scars, showing a gradual differentiation (Fig. 26).

3.2.3. Time point 6 h

3.2.3.1. General. Most of the newly transformed sporocysts had shed their ciliated plates and lost their terebratorium (Figs. 27–29). Young sporocysts measured between 47 µm up to 90 µm. Many of them were

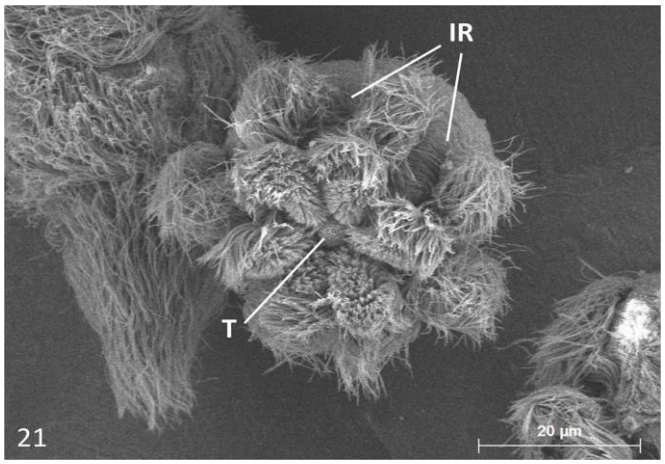

Fig. 21. Scanning electron micrographs of 4 h transforming miracidia, details of the apical region × 1500. Remnants of ciliated plates are concentrated in the apical region were the terebratorium (T) is hidden. Proliferative intercellular ridge (IR) is visible between ciliated plates.

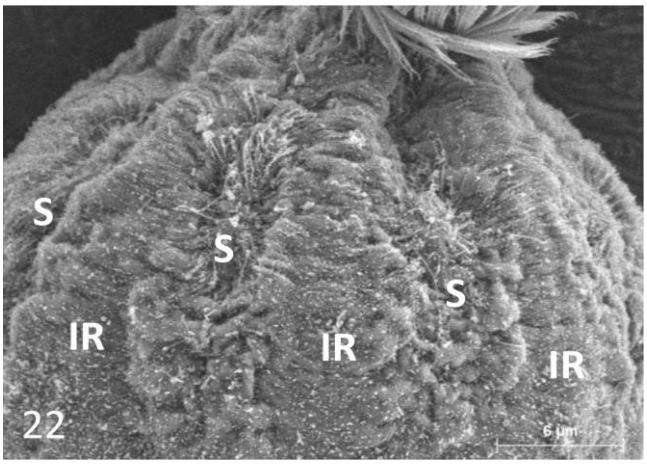

Fig. 22. Scanning electron micrographs of 4 h transforming miracidia of *S. mansoni*. 22 Focus on the interridge (IR) proliferation in between scars (S) due to the loss of ciliated plates × 4000.

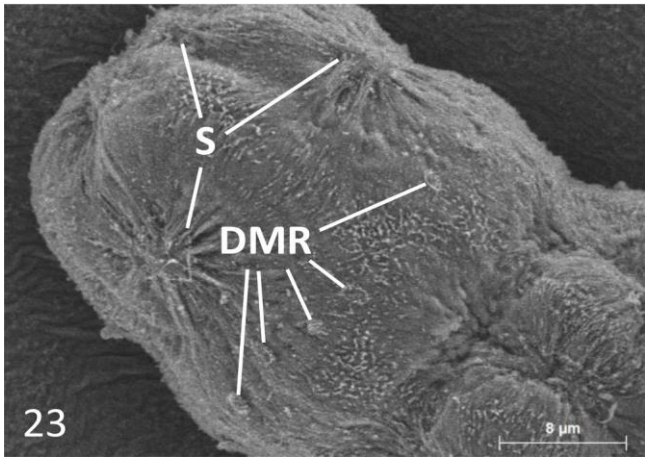

Fig. 23. Details of the tegument scars (S) × 3000. At 4 h of transformation, the organism shows typical star-like scars in the posterior section of the animal, degenerating multiciliated receptors (DMR) in the limit between the last and the second third of the transforming miracidium. still contracted at this stage (Fig. 28).

3.2.3.2. Apex. Some individuals exhibited a remnant terebratorium. Most of the sporocysts had no terebratorium left and "shreds" were present at the apex but not clearly noticeable on all the individuals (Figs. 30 and 31) as well as an apex scar due to the loss of the apical papilla (Figs. 30 and 31). Post-miracidium lateral papillae are free and visible and seem covered by the same tegument than the whole miracidium body. Multiciliated receptors can also be seen near the lateral papillae at this time point (Figs. 30 and 31).

3.2.3.3. Tegument. The tegument is close to the end of its differentiation, although cicatricial furrows are still presents (Figs. 30 and 32). The intercellular ridge is now quite extended between scars and microvilli are noticeable on the tegument surface. The detail of a detached ciliated plate is presented in Fig. 33 despite ciliated plates started to detach earlier.

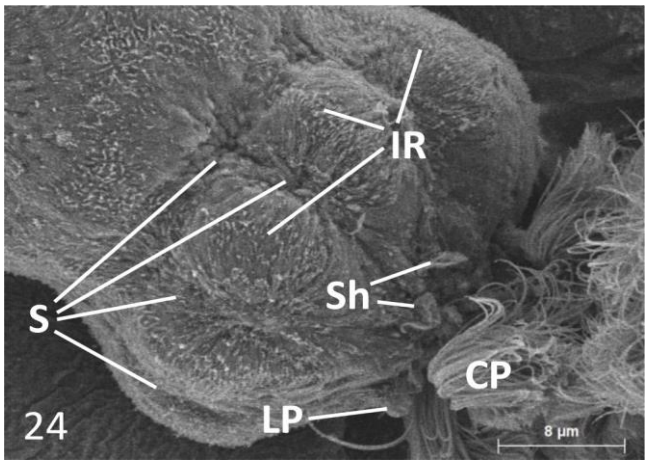

Fig. 24. Upper in the animal, furrow-like scars (S) are visible × 3000. The proliferative interplate tegument (IR) can be seen. The presence of a lateral papilla (LP) indicates the top of the animal as well as "shreds" (Sh) appearing, probably caused by the loss of the terebratorium, those structures being noticeable at a later time point. Remnants ciliated plates (CP) are also visible.

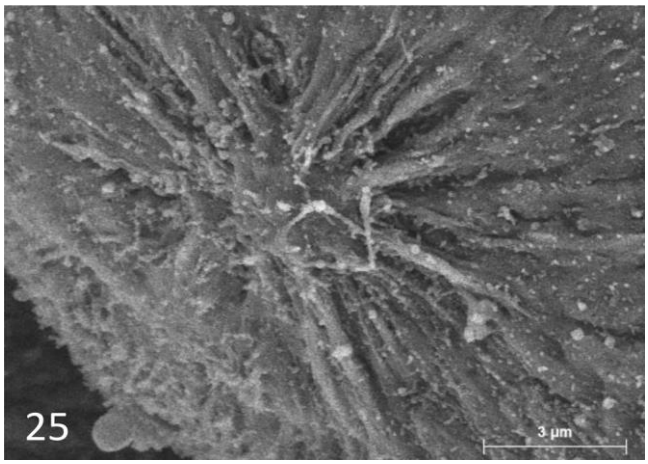

Fig. 25. Details of the star-like scars (posterior area of the organism) × 9000.

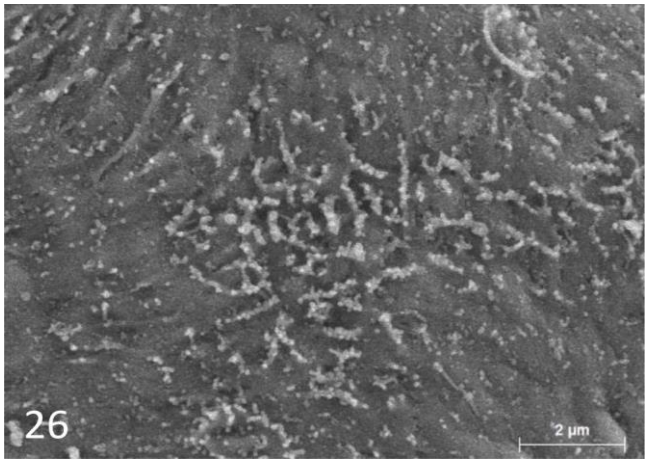

Fig. 26. Magnification of the proliferative new tegument coming from the intercellular ridge × 10,000.

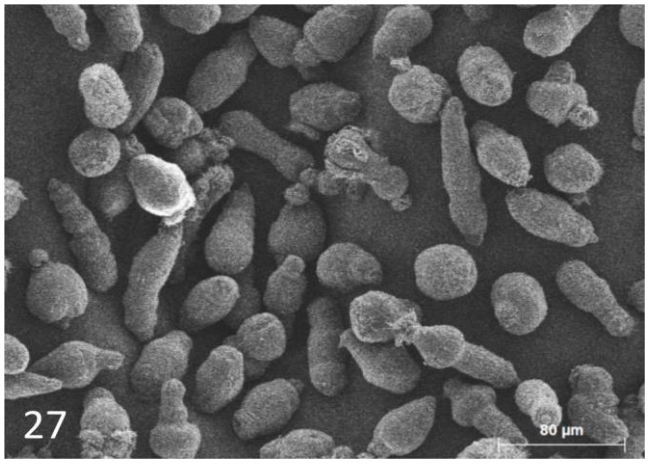

Fig. 27. Scanning electron micrographs of 6 h transforming miracidia. 27 Transforming miracidia of *S. mansoni* (6 h) × 300.

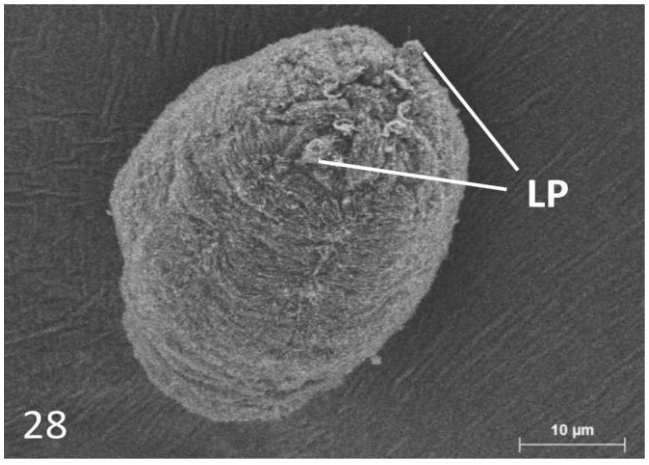

Fig. 28. Focus on single transforming individual × 2000, lateral papillae (LP) can be noticed in the apical region.

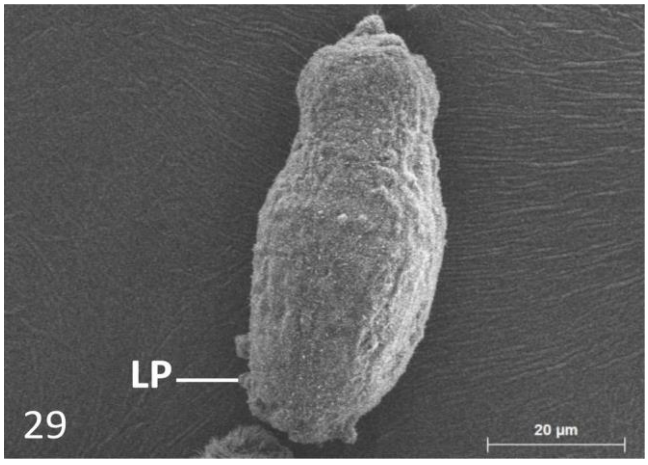

Fig. 29. Focus on single transforming individual × 1300, lateral papillae (LP) can be noticed in the apical region.

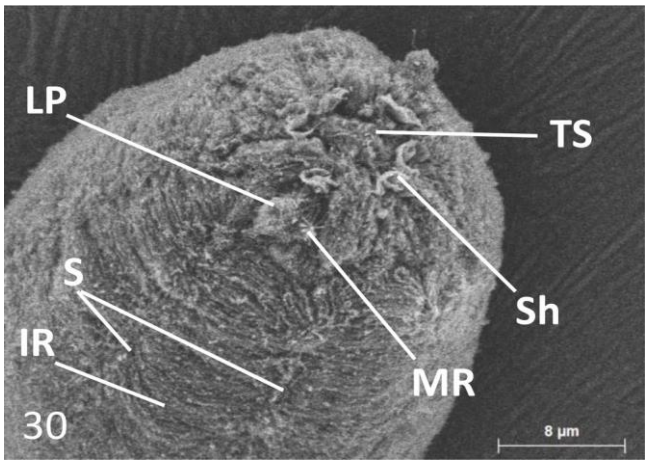

Fig. 30. Scanning electron micrographs of 6 h transforming miracidia of *S. mansoni*. **30** Magnification of the apical region of a young sporocyst × 3000, lateral papillae (LP) are visible in the apical region of the organism, shreds (Sh) around the scar provoked by the loss of the terebratorium (TS) can be seen at the apex. Near to lateral papillae can be noticed multiciliated receptors (MR) and on the body, scars (S) due to the loss of ciliated plates and proliferating interplate ridge (IR) can still be seen.

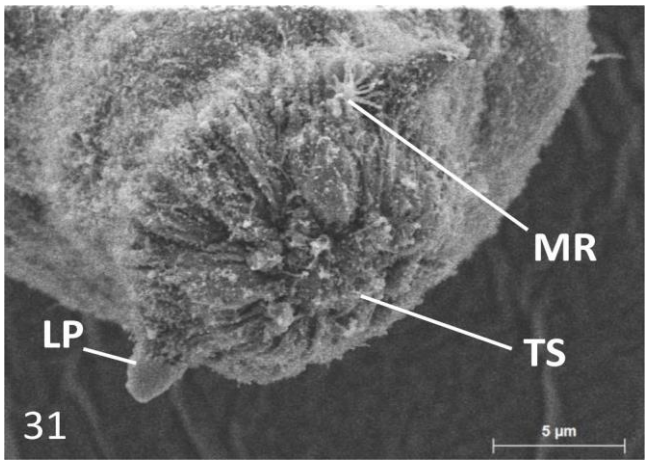

Fig. 31. Focus on the apical region × 5000 where can still be seen a multiciliated receptor (MR), lateral papillae (LP) and the remnant scar due to the loss of terebratorium at the apex (TS).

3.2.4. Time point 12 h

3.2.4.1. General. Sporocysts continued to elongate, measuring about 100 µm for the longest individuals, some ciliated plates and apical papillae (terebratoria) were visible among the individuals (Figs. 34–36).

3.2.4.2. Apex. Multiciliated papillae were visible at the apex
(Figs. 37–39) close to lateral papillae. While usually present in pairs, the individual observed had three of those (Figs. 35, 37 and 38). Terebratorium is often lost (Fig. 36) but can sometimes be noticed (Figs. 35 and 37), the apical region is less flat than at 6 h and start to protrude between lateral papillae (Fig. 37). Microvilli are now clearly visible on lateral papillae and in the whole apical region.

3.2.4.3. Tegument. The entire organism is covered with microvilli (Figs. 40–43), previous scars originating from the loss of ciliated plates are still visible (Fig. 40) and the previous intercellular ridge now constitutes the newly formed syncytial tegument (Fig. 40). Remnants of degenerated multiciliated receptors can still be observed in the medial section (Figs. 41–43).

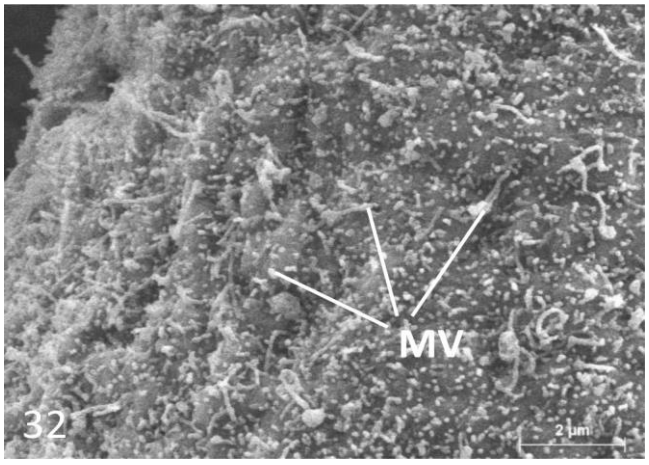

Fig. 32. Details of the tegument surface × 10,000, microvilli (MV) can be noticed as well as the rugous aspect of this newly formed tegument. The greatest part of the animal is covered by this kind of tegumentary surface.

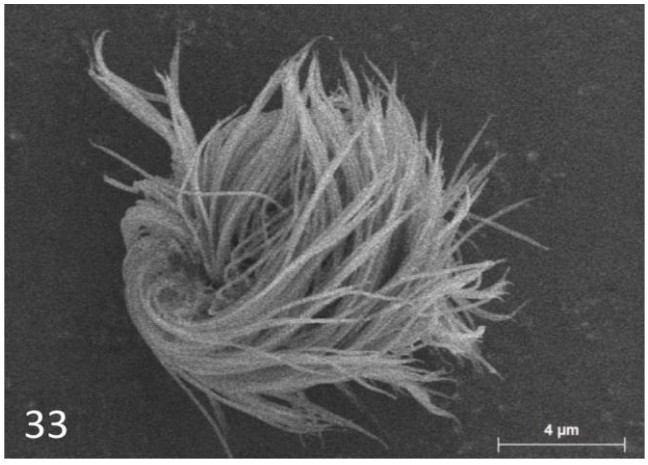

Fig. 33. Details of a detached ciliated plate × 6000, ciliated plates are round- shaped after detachment, this typical shape can still be observed through an optical microscope.

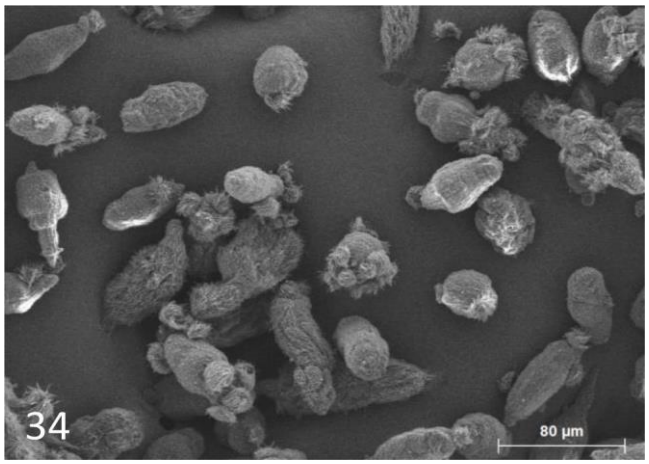

Fig. 34. Scanning electron micrographs of 12 h transformed sporocysts. 34 Transforming sporocysts of *S. mansoni* (12 h) × 300.

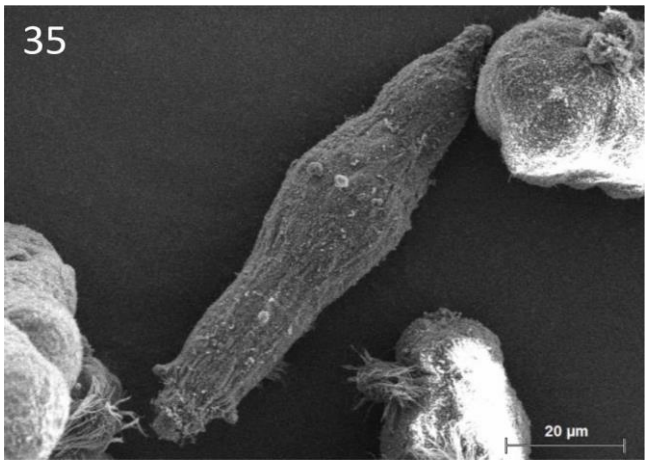

Fig. 35. Focus on single transforming individual × 1100.

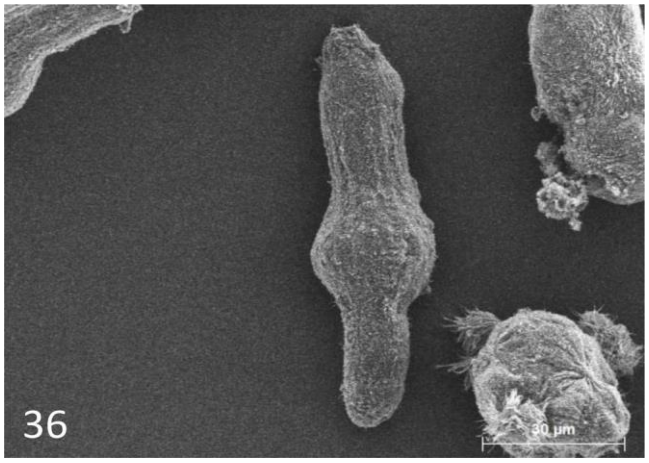

Fig. 36. Focus on single transforming individual × 900.

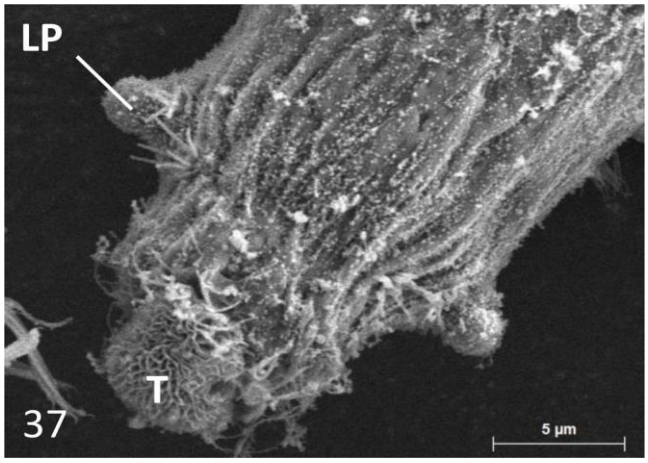

Fig. 37. Scanning electron micrographs of 12 h transforming miracidia of *S. mansoni*. 37 Details of the apical region of a 12 h transformed sporocyst × 5000, lateral papillae (LP) are visible, terebratorium (T) can sometimes remain in place as observed on the picture.

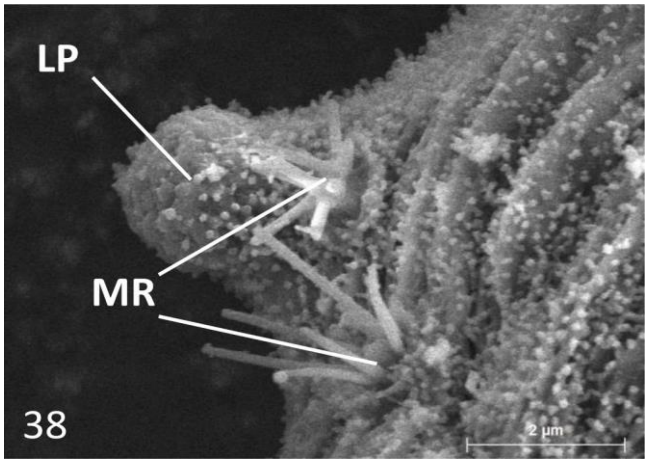

Fig. 38. Magnification of a lateral papilla (LP) × 15,000, multiciliated receptors (MR) are visible around the area of the lateral papillae.

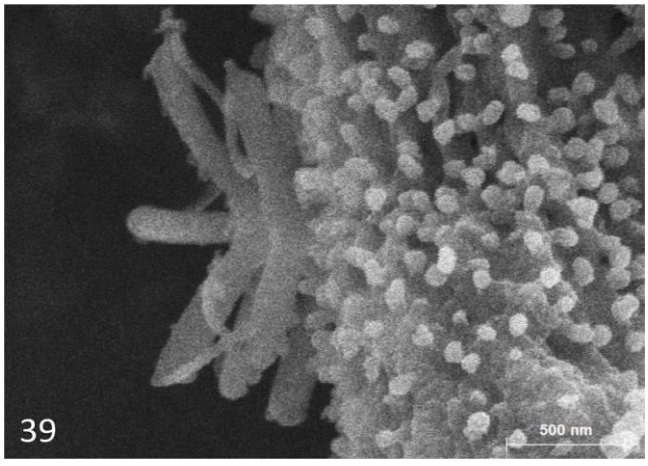

Fig. 39. Details of a multiciliated receptor × 45,000.

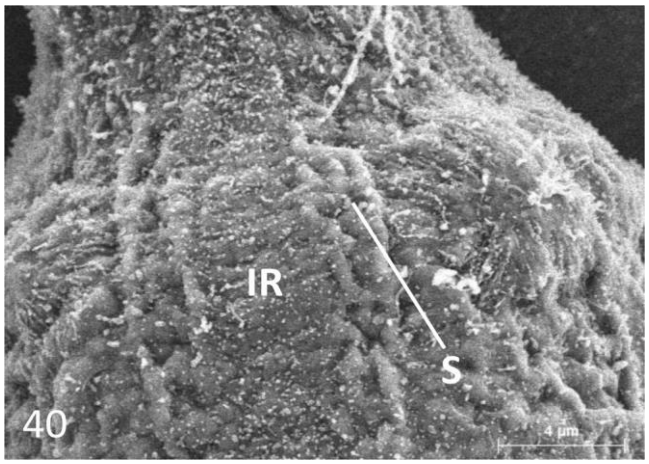

Fig. 40. Scanning electron micrographs of 12 h transforming miracidia tegument of *S. mansoni*. **40** Details of a 12 h sporocyst mid-section tegument × 6000, the proliferative intercellular ridge (IR) is still visible between remnant scars (S).

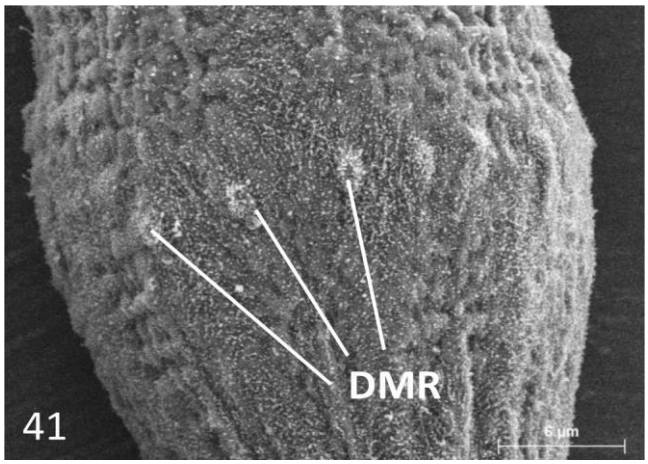

Fig. 41. Mid-section of a sporocyst × 4000 showing residual degenerated multiciliated receptors (DMR).

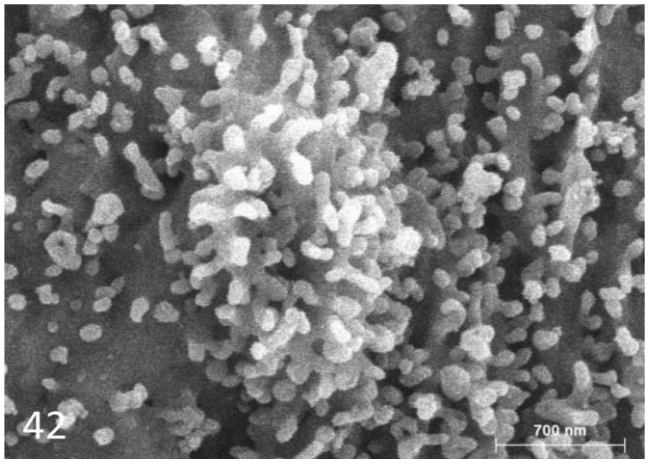

Fig. 42. Focus on a degenerated multiciliated receptor (DMR) × 35,000.

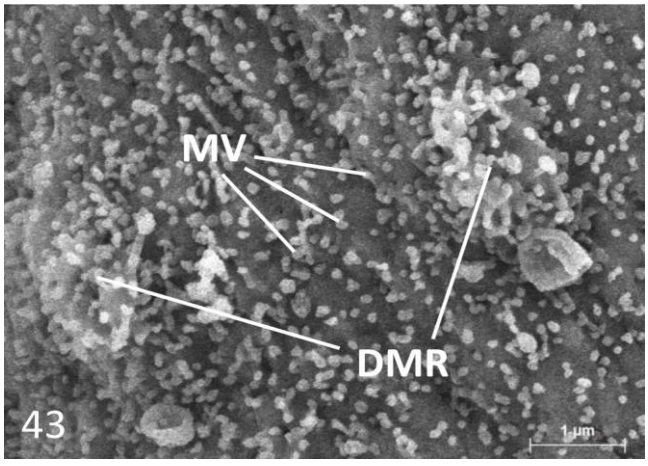

Fig. 43. Focus on degenerated multiciliated receptors (DMR) and microvilli (MV) × 18,000.

3.2.5. Time point 24 h

3.2.5.1. General. Sporocysts are longer and less contracted compared to 12 h of transformation. Their shape is more cylindrical and continues to elongate (Figs. 44 and 45).

3.2.5.2. Apex. The apex tegument seems more homogenous since terebratorium scar is less noticeable at this time point (Figs. 46 and 47). Multiciliated receptors are still visible, always close to the lateral miracidial papillae which are covered with microvilli (Figs. 48 and 49). Terebratorium has completely disappeared from any observed individuals at this stage.

3.2.5.3. Tegument. Microvilli cover the entire body of the sporocysts, scars are now less visible and hard to distinguish on the sporocyst surface tegument (Figs. 45 and 46).

3.2.6. Time point 48 h

3.2.6.1. General. Sporocysts are now longer, no more ciliated plates are present, individuals measure between 85 and 110 µm long for 25 µm width in the mid-section, 8 µm width at the apex. Sporocysts in culture exhibit undulating movements resulting in variation of lengths and widths for each individual upon fixation and therefore making it difficult to measure. (Figs. 50–52).

3.2.6.2. Apex. The apex is more and more protruding in front of lateral papillae (Fig. 53), no terebratorium is noticed at 48 h time point. A depression can be observed at the apex and could constitute a potential birth pore (Figs. 53 and 54). Apical multiciliated receptors near the lateral papillae can still be observed (Fig. 55), lateral papillae still remaining from the miracidium stage are now entirely covered by microvilli (Fig. 56).

3.2.6.3. Tegument. Microvilli are denser and longer making harder to observe the underlying surface of the syncytial tegument (Figs. 57–60). A lot of budding and free vesicles can be observed at the surface of the sporocyst tegument (Figs. 57 and 58). Two pore-like structures can often be observed in the middle of the sporocyst body, symmetrically located on both sides of the anteroposterior axis, those probably corresponding to newly formed excretory pores (Figs. 59 and 60).

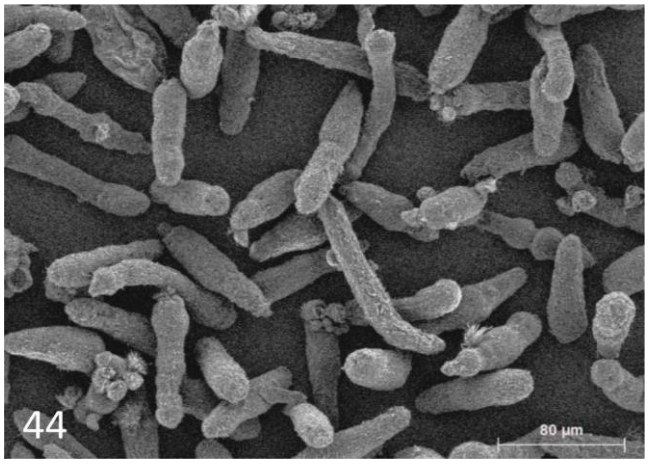

Fig. 44. Scanning electron micrographs of 24 h transformed sporocysts. 44 Scanning electron micrograph of 24 h transformed population (× 300).

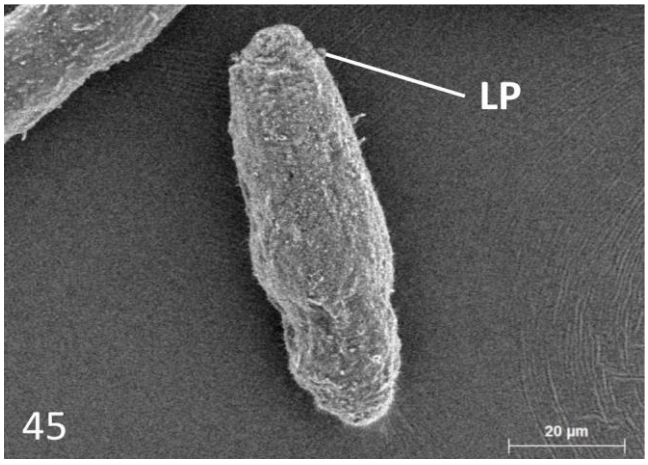

Fig. 45. Focus on a single transforming individual, lateral papillae (LP) at the apex help to orientate the sporocyst (× 1100).

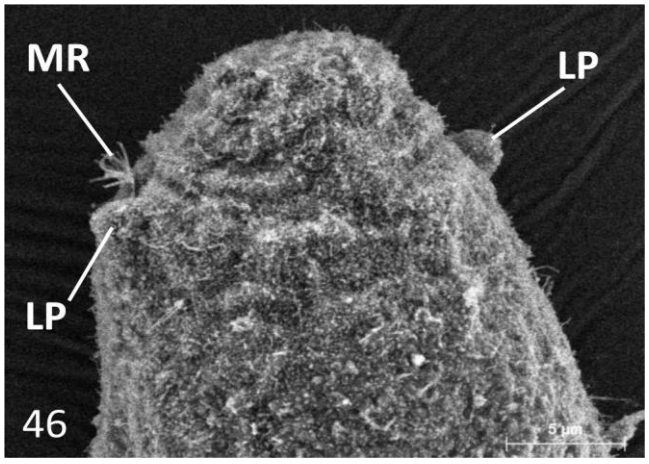

Fig. 46. Scanning electron micrographs of 24 h transforming sporocysts of *S. mansoni*. 46 Details of the apical region of a 24 h transformed sporocyst × 4500, lateral papillae (LP) are visible, as well as an associated multiciliated receptor (MR).

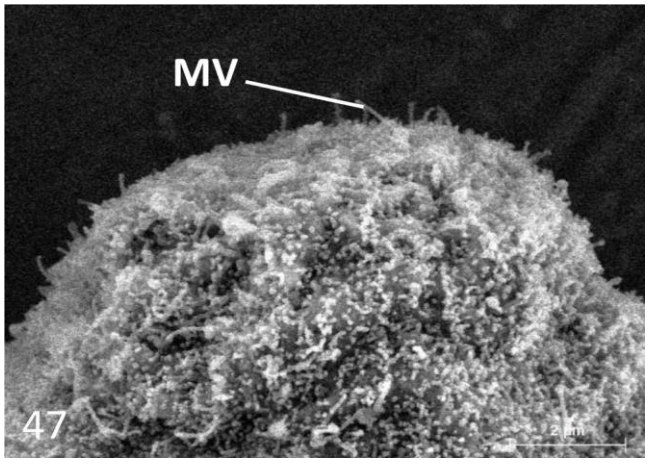

Fig. 47. Details of the apex of a 24 h-transformed sporocyst, microvilli can be observed (MV) × 11,000.

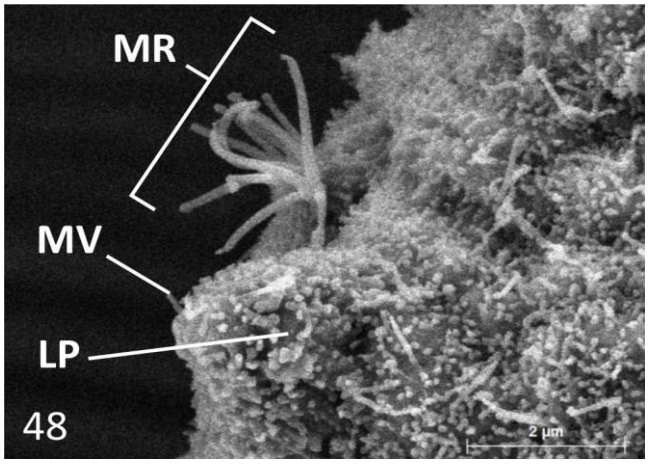

Fig. 48. Magnification of a lateral papilla (LP) × 15,000, multiciliated receptors (MR) is visible in the area of the lateral papillae.

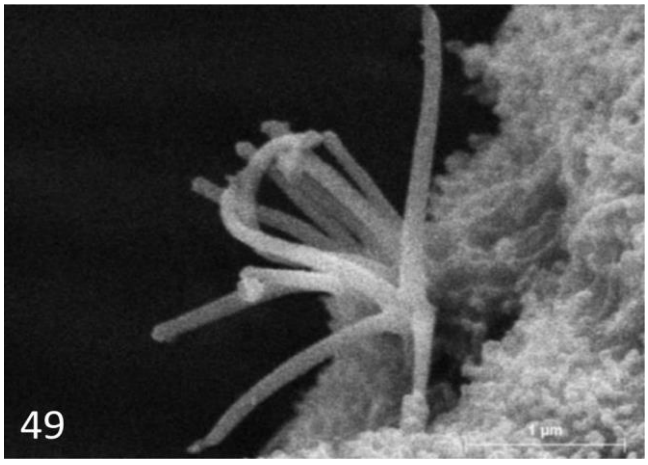

Fig. 49. Details of a multiciliated receptor × 30,100.

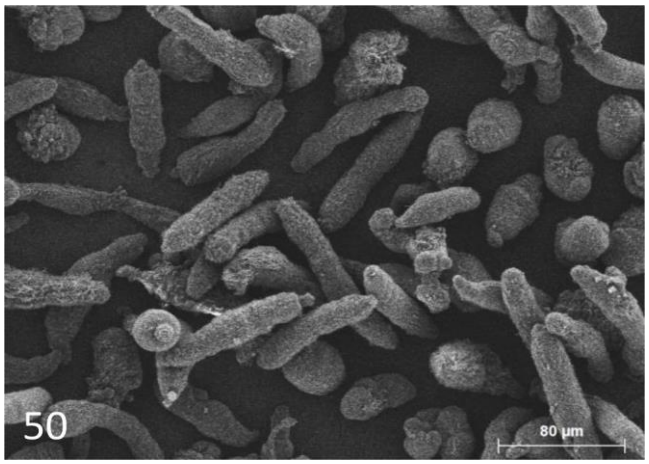

Fig. 50. Scanning electron micrographs of 48 h transformed sporocysts. 50 Sporocysts of *S. mansoni* (48 h) × 300.

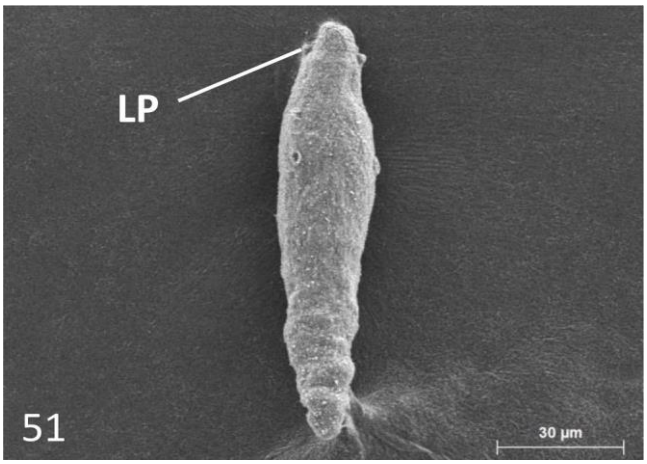

Fig. 51. Focus on single individuals × 800.

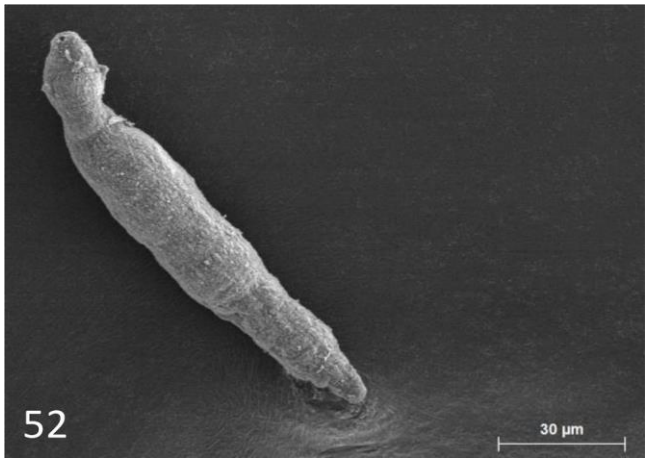

Fig. 52. Focus on single individuals × 800.

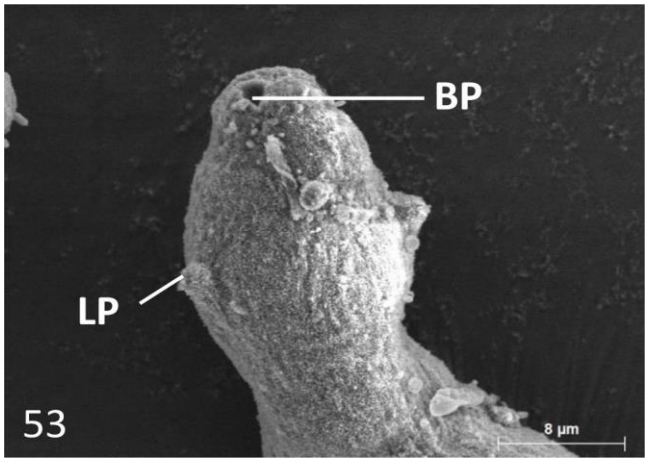

Fig. 53. Details of the apical area of a 48 h sporocyst × 3000, a depression is often seen at the apex of the organism, this depression could probably be a birth pore, allowing daughter sporocysts further passage (BP), lateral papillae are still noticeable (LP).

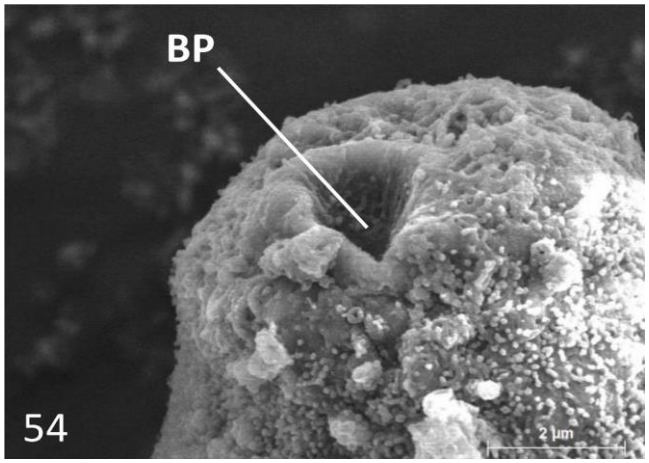

Fig. 54. Focus on the apical depression of the sporocyst × 13,000.

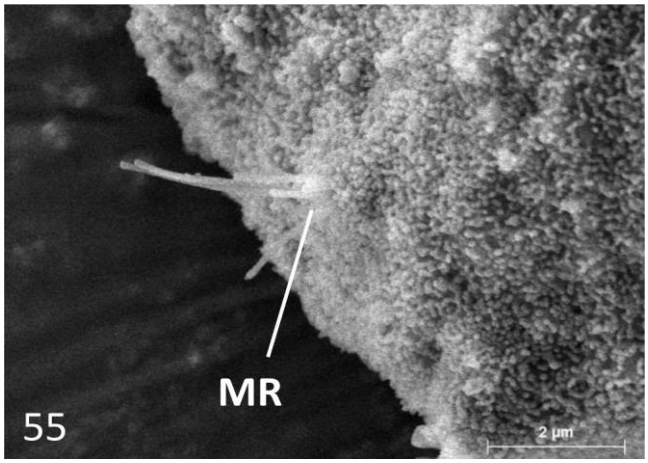

Fig. 55. Focus on a multiciliated receptor (MR) close to a lateral papilla × 13,000.

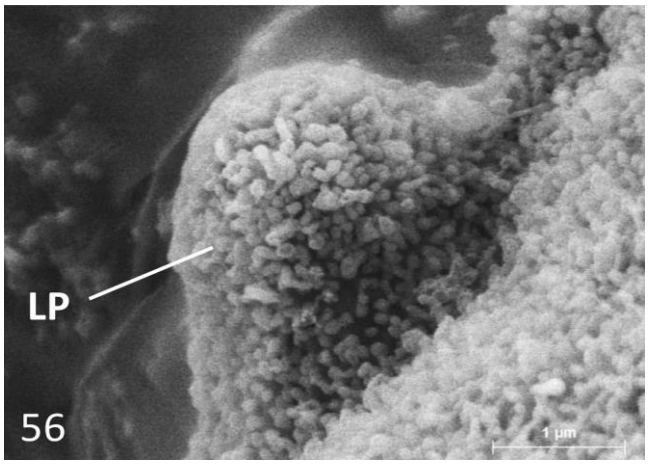

Fig. 56. Details of an apical lateral papilla (LP) covered by microvilli × 25,000.

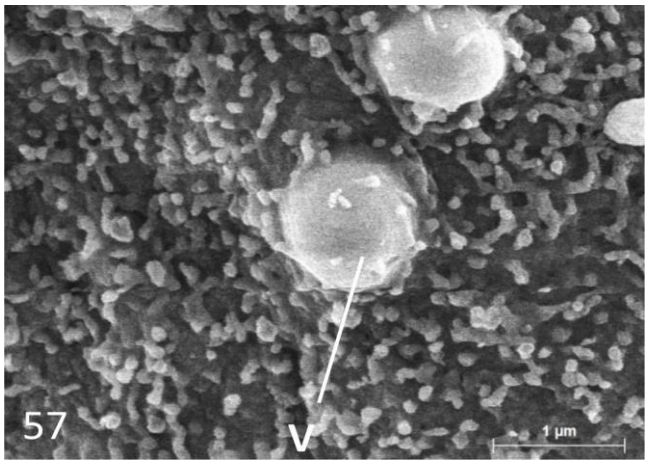

Fig. 57. Scanning electron micrographs of 48 h sporocyst tegument of *S. mansoni*. **57** Budding of vesicles × 25,000, vesicles (V) are often seen emerging from the sporocyst surface.

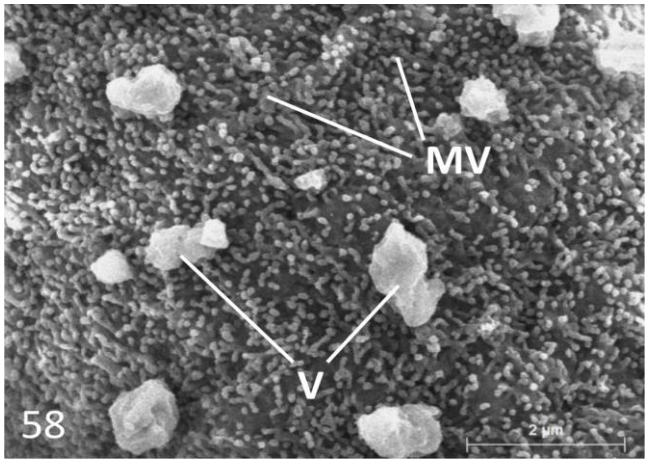

Fig. 58. Details of the tegument × 15,000 showing vesicles (V) and microvilli (MV).

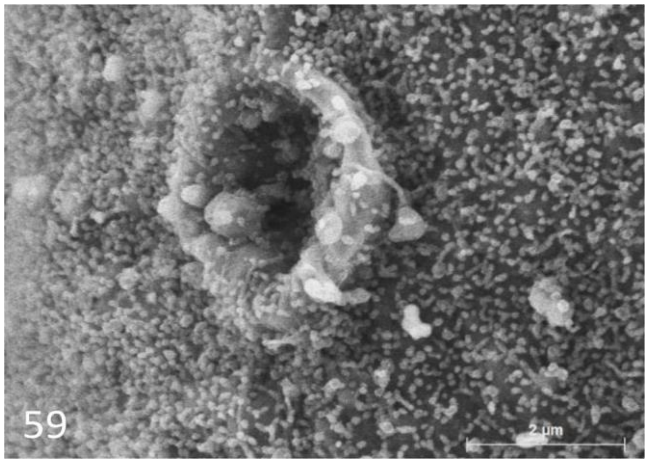

Fig. 59. Tegumental pore-like structure observed at the surface of sporocysts × 15,000.

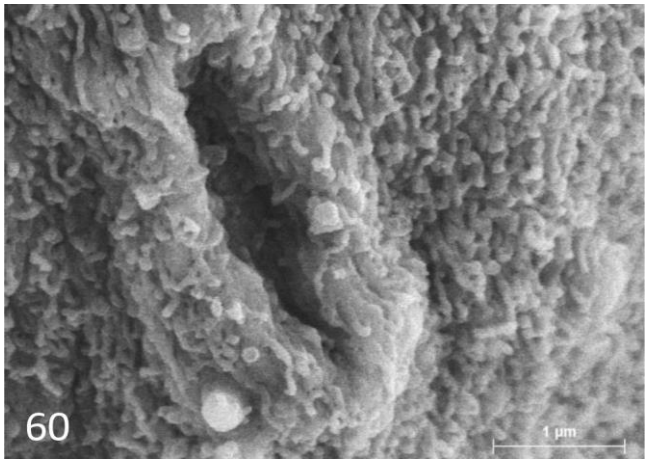

Fig. 60. Tegumental pore-like structure observed at the surface of sporocysts × 25,000.

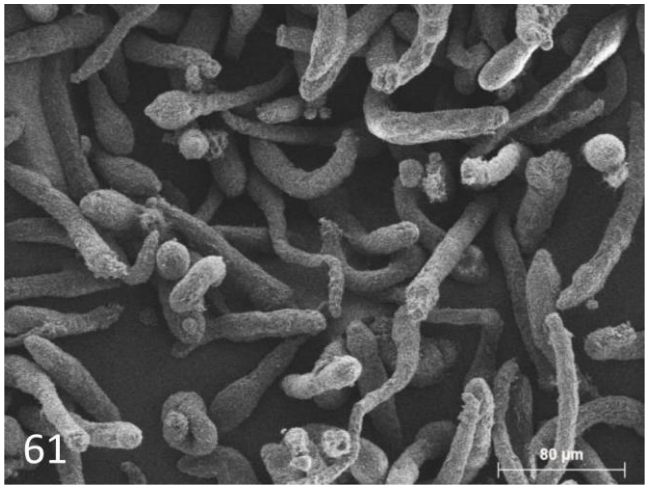

Fig. 61. Scanning electron micrographs of 97 h transformed sporocysts. 61 Sporocysts of *S. mansoni* (97 h) × 300.

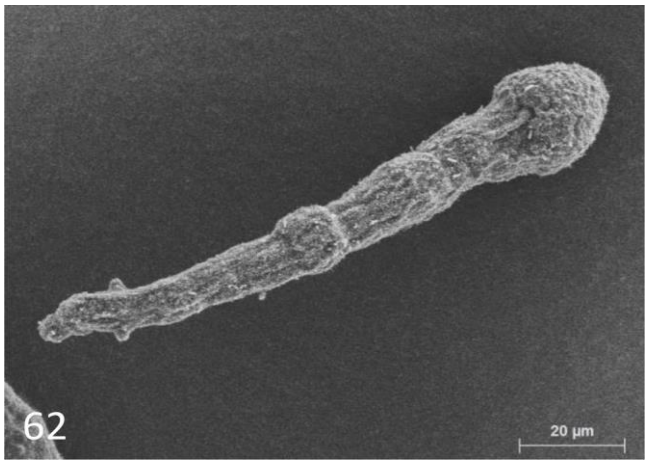

Fig. 62. Focus on single individual × 1000.

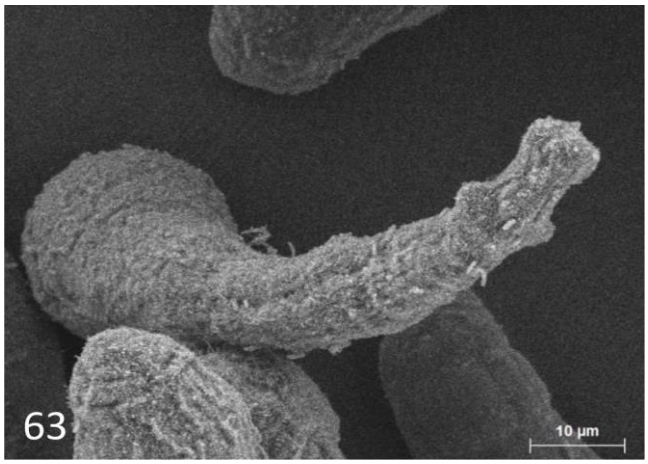

Fig. 63. Focus on single individual × 1800.

3.2.7. Time point 97 h

The description of the sporocyst morphology at 97 h time point is identical to the morphological structures observed at 120 h of transformation thus those data have not been described herein.

3.2.7.1. General. Sporocysts keep elongating, individuals are longer, reaching 120 µm (Figs. 61–63). Dimensions of the sporocysts can vary depending on the contraction or relaxation state of the organisms. At this time point, sporocysts displayed a vermiform (worm-shaped) body and can be find coiled and sometimes with a bulbar swelling on the posterior end (Figs. 62 and 63).

3.2.7.2. Apex. The apex is more protruded compared to previous time point and can protrude from 10 to 20 µm in front of lateral papillae. Multiciliated receptors are now on this protrusion and farther from the lateral papillae. On the apex, depressions can be seen (Fig. 64) probably a birth pore, but are not systematically observed for all individuals.

3.2.7.3. Tegument. The tegument is still covered with microvilli, but with a higher density (Figs. 65 and 66), at this level no important changes were noticed compared to 48 h time point.

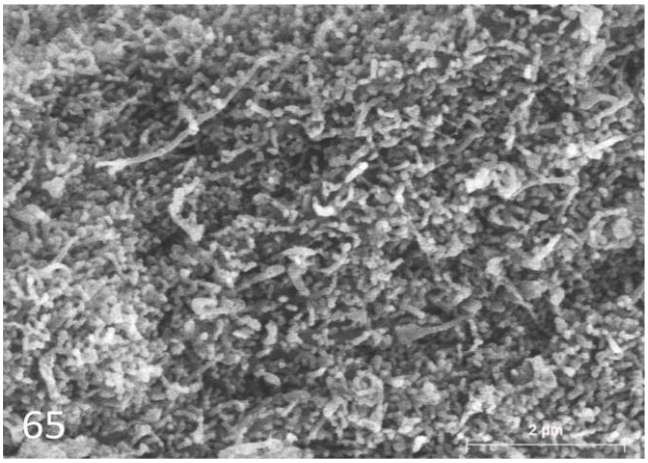

Fig. 64. Scanning electron micrographs of 97 h transformed sporocysts (details). 64 Focus on single individual apical region × 5000, lateral papillae (LP) are still present, multiciliated receptors (MR) are visible, the apex is prolonged, and depressions are sometimes seen at the apex of the sporocysts, probably a birth pore (BP).

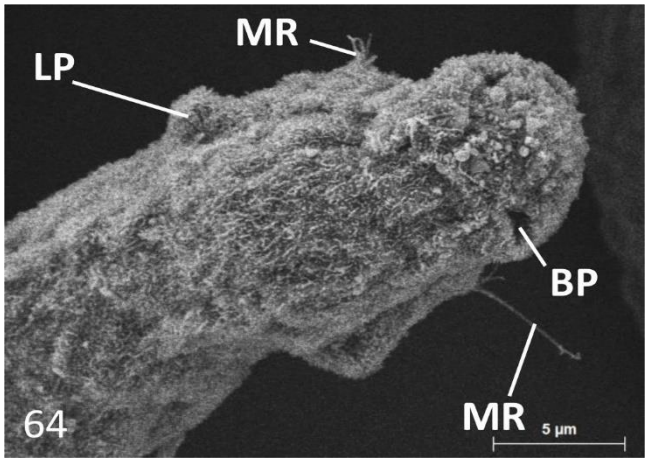

Fig. 65. Scanning electron micrograph of 97 h sporocyst tegument of *S. mansoni* × 15,000.

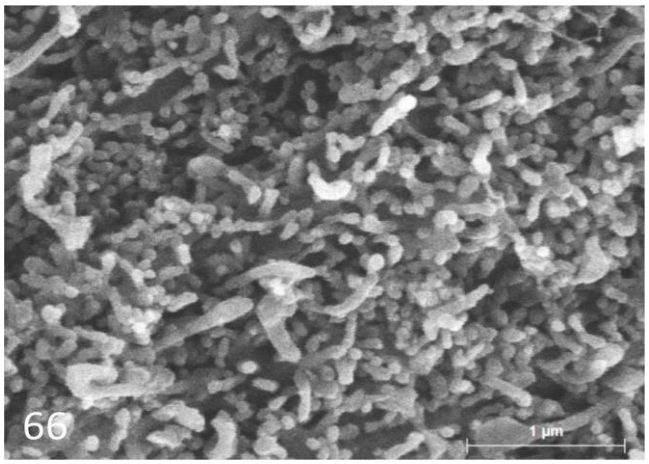

Fig. 66. Scanning electron micrograph of 97 h sporocyst tegument of *S. mansoni* × 30,000.

4. Discussion

This present work, to our knowledge is the first study dedicated to describe the tegument ultrastructure changes occurring during the span of a complete *in vitro* transformation of miracidia to fully transformed sporocysts of *S. mansoni*.

This miracidium to sporocyst transformation depends on deep apical and tegument body changes. The first important modification of the tegument surface is the loss of ciliated plates due to the proliferation of the interplate ridge (Dunn and Yoshino, 1988), this loss being sequential from posterior to anterior plates (Samuelson and Caulfield, 1985; Daniel et al., 1992). Terebratorium is often lost after the loss of apical ciliated plates but can remain idiosyncratically after 12 h of *in vitro* transformation. It is relevant to notice the fact that populations of transforming miracidia are still heterogenous after 12 h of *in vitro* transformation. Some larvae still exhibited one or more plates on their surface between 12- and 24 h of transformation but all the sporocysts have lost their ciliated plates between 24 and 48 h of transformation.

4.1. Apical region

The terebratorium exhibited the same structures described previously in the literature (Koie and Frandsen, 1976; Pan, 1980; Eklu-Natey et al., 1985; Kruger and Hamilton-Attwell, 1988), with uniciliated and multiciliated receptors (sometimes called “ciliated pit” by authors). However we did not notice “rod-shaped bodies”, probably representing adherent bacteria to parasite surface as mentioned by Koie and Frandsen (1976). No bacteria were seen during our observations at the miracidium stage nor before 48 h time point. We observed very similar receptor pattern on the terebratorium as described by Eklu-Natey and collaborators for *S. japonicum i.e.*, four multiciliated receptors laterally flanked two by two, both framed by four uniciliated receptors, the terebratorium surmounted by two central uniciliated receptors (Eklu-Natey et al., 1985). Sometimes, one supernumerary multiciliated receptor could be detected. Their exact biological function is still not completely understood, and it is unknown whether those ciliated receptors can act as mechanoreceptors (either rheo- or tangoreceptors) or chemoreceptors. These lacks in the biological function of multiciliated receptors will deserve further investigation, however in the present study, as in the previous works, solely their morphologies and structures have been included (Kinoti, 1971; Pan, 1980).

Lateral gland apertures (Eklu-Natey et al., 1985) were noticed, often containing amorph structure, probably secretion products (Pan, 1980). Barb-shaped cilia were noticed back from the apical papilla, shorter than the locomotory ciliature. Due to the shape of these cilia, a potential role in miracidium attachment and penetration in mollusk tissue can be hypothesized.

Metamorphosis of the miracidium induces ciliated plates detachment causing the exposition of median and apical multiciliated receptors anchored in the interplate ridge, as well as lateral papillae. It is interesting to notice the persistence of lateral papillae through the entire metamorphosis process. However, it is unknown if those papillae remain functional or not. A probable function of “depth sensor” for those lateral bulbous papillae was hypothesized for the miracidium stage (Pan, 1980). The overlying of the papillae by microvilli let think to a loss of function of these miracidial structures through the transformation process. It is intriguing to notice that the apical multiciliated receptors not associated with the terebratorium do not degenerate. In contrast to the median multiciliated receptors that degenerate during the first 12 h of transformation. The apical multiciliated receptors persist even after 120 h of transformation. Those multiciliated receptors are often present in pair, but a supernumerary receptor can also be observed in exceptional cases.

At the same time, the apex protruded throughout the transformation process. Regarding the apical depression, some evidence led us to propose that this depression acts as a birth pore as described by Jourdane and Mingyi, permitting daughter sporocysts (secondary sporocysts) to be released from mother sporocysts (primary sporocysts) without physical injuries through mother-sporocysts body wall (Jourdane and Mingyi, 1987). The presence of a birth pore could be consistent with the fact that *in vitro* maintained mother sporocysts were able to emit daughter sporocysts during several weeks (Yoshino and Laursen, 1995; Ivanchenko et al., 1999). However, the presence of a birth pore in mother-sporocysts has never been demonstrated, despite observations of a birth pore in *S. mansoni* daughter sporocysts for release of the cercariae (Fournier and Th´eron, 1985).

4.2. Tegument

Changes of the tegument begin by the proliferation of the intercellular (or interplate) ridge. This proliferation starts before ciliated plates loss and induce their detachment (Yoshino et al., 2016). Typical scars can be noticed consecutive to this detachment, furrow-like in the anterior part and star-like scars on the posterior part of the sporocyst body. Scars remain after 12 h of transformation. The newly appearing tegument differentiates by emergence of microvilli (Basch

and DiConza, 1974). Median multiciliated receptors start to degenerate at 4 h of transformation. Microvilli were denser through the transformation process and covered the whole surface of the organism. Pores were noticed on the mid-section for some individual sporocysts after 48 h of transformation. When seen, those structures were always present in pair, probably constituting excretory pores with a different shape than the ones of the miracidium. Sporocysts continued to grow after 48 h, the apical region protruding more and more and sporocysts sometimes forming a bulbar swelling on the posterior end or a spiral twist, as previously described (Basch and DiConza, 1974).

Tegument microvilli start to appear after about 6 h of transformation and become denser and denser throughout the transformation, increasing the exchange surface. The entire body of the sporocyst is covered with microvilli excepted the two apical multiciliated receptors emerging. On the tegument, some large vesicles emerging and free vesicles were observed, with a size between 500 nm and 1,5 µm. Despite host immunomodulation passing through direct exocytosis of immunomodulatory substances among excretory/secretory products for the sporocysts (Dunn and Yoshino, 1988; Yoshino and Lodes, 1988; Lodes and Yoshino, 1989; Guillou et al., 2007), it is not excluded that the observed extracellular vesicles can have a role in host immunomodulation as for example through miRNA transport which is a reported phenomenon in the adult stage of schistosomes (Bischofsberger et al., 2020; Meningher et al., 2020; Li et al., 2022) or through other protein compounds released in extracellular vesicles such as Heat Shock Proteins (Acharya et al., 2021).

Improvement of scanning electron microscopy technologies through the past forty years coupled to a CO_2 critical point drying method (osmium tetroxide post-fixation of biological samples is useless in scanning electron microscopy) permitted to obtain fairly good quality images. It is important to precise, the presented transformation mechanism occurs in an *in vitro* context, the remaining of terebratorium after 6 h of transformation for some individuals did not potentially happen *in vivo*. The same is true for the persistency of some ciliated plates after this period or the quick renewing of the tegument which is slower *in vitro* (Dunn and Yoshino, 1988). Moreover, there is no mechanical help for miracidia to detach from the plates neither from the terebratorium unlike what happens during the *in vivo* penetration and transformation. Nevertheless, the presented work aims to raise an awareness of the morphological and tegument variations between different durations of *in vitro* miracidium transformation. This surface variation could be followed by biochemical changes that could impact experimental strategies such as exposure of the parasites with different molecular agents. Thus, in the context of snail-parasite interactions, this work calls for further functional studies using SEM markers (*e. g.* gold tagged proteins) for coupled molecular and ultrastructural approaches. The evolution of SEM techniques has allowed us to obtain higher resolution images of miracidial and sporocyst structures, which will also provide reference images for future applications such as analysis effect of host immune factors, or exposure to anti-parasitic compounds on sporocyst syncytial tegument potentially interfering on transformation processes (de Carvalho Augusto et al., 2020).

Funding

This work was funded by ANR AeroSNAIL (number ANR-19CE11- 0016).

Declaration of Competing Interest

The authors declare that they have no known competing financial interests or personal relationships that could have appeared to influence the work reported in this paper.

CRediT authorship contribution statement

Pierre Poteaux: Conceptualization, Methodology, Investigation, Resources, Data curation, Writing – original draft, Writing – review & editing, Visualization, Project administration. **Benjamin Gourbal:** Writing – original draft, Writing – review & editing. **David Duval:** Writing – original draft, Writing – review & editing, Supervision, Funding acquisition.

Data availability

Data will be made available on request.

Acknowledgment

The authors would like to thank Yonko Gorand from the centre de Caract´erisation de la matiere C2M PROMES/CNRS for introducing to the ` use of a scanning electron microscope and its specific sample preparation, including the critical point drying method. Thanks to Dr Julien Portela from ParaDev company for the maintenance of mollusc and parasite strains. We thank the anonymous reviewers for their careful reading of our manuscript and their insightful suggestions.

This study is set within the framework of the “Laboratoire d’Excellence (LabEx)” TULIP (ANR-10-LABX-41).

References

Acharya, S., Da'dara, A.A., Skelly, P.J., 2021. Schistosome immunomodulators. PLoS Pathog. 17 (12), e1010064 https://doi.org/10.1371/journal.ppat.1010064.

Amara, R.O., et al., 2018. Praziquantel–lipid nanocapsules: an oral nanotherapeutic with potential *Schistosoma Mansoni* tegumental targeting. Int. J. Nanomed. 13, 4493–4505. https://doi.org/10.2147/IJN.S167285.

Araújo, H.D.A., et al., 2019. Usnic acid potassium salt from Cladonia substellata (Lichen): synthesis, cytotoxicity and *in vitro* anthelmintic activity and ultrastructural analysis against adult worms of *Schistosoma mansoni*. Acta Trop. 192, 1–10. https://doi.org/ 10.1016/j.actatropica.2018.12.024.

Araújo, H.D.A., et al., 2020. *In vitro* activity of usnic acid potassium salt against different developmental stages of *Schistosoma mansoni*: an ultrastructural study. Acta Trop. 201, 105159 https://doi.org/10.1016/j.actatropica.2019.105159.

Basch, P.F., DiConza, J.J., 1974. The miracidium-sporocyst transition in *Schistosoma mansoni*: surface changes *in vitro* with ultrastructural correlation. J. Parasitol. 60 (6), 935–941. https://doi.org/10.2307/3278518.

Bender, R.C., et al., 2002. *Schistosoma mansoni* sporocysts in culture: host plasma hemoglobin contributes to *in vitro* oxidative stress. J. Parasitol. 88 (1), 14–18. https://doi.org/10.2307/3285384.

Bischofsberger, M., et al., 2020. Pathogen-host interaction mediated by vesicle-based secretion in schistosomes. Protoplasma 257 (5), 1277–1287. https://doi.org/ 10.1007/s00709-020-01515-y.

Brandao-Bezerra, L., et al., 2019. Long-term ethanol intake causes morphological ˜ changes in *Schistosoma mansoni* adult worms in mice. Exp. Parasitol. 203, 30–35. https://doi.org/10.1016/j.exppara.2019.05.010.

Campos, Y.R., et al., 2002. Genetic variability of the main intermediate host of the *Schistosoma mansoni* in Brazil, Biomphalaria glabrata (Gastropoda: planorbidae) assessed by SSR–PCR. Acta Trop. 83 (1), 19–27. https://doi.org/10.1016/S0001- 706X(02)00051-7.

Catalano, S., et al., 2020. Multihost transmission of *Schistosoma mansoni* in Senegal, 2015–2018˙. Emerging Infect. Dis. 26 (6), 1234–1242. https://doi.org/10.3201/ eid2606.200107.

Chernin, E., 1963. Observations on hearts explanted *in vitro* from the snail australorbis glabratus. J. Parasitol. 49 (3), 353–364. https://doi.org/10.2307/3275797.

Dalton, J.P., Skelly, P., Halton, D.W., 2004. Role of the tegument and gut in nutrient uptake by parasitic platyhelminths. Can. J. Zool. 82 (2), 211–232. https://doi.org/ 10.1139/z03-213.

Daniel, B.E., Preston, T.M., Southgate, V.R., 1992. The *in vitro* transformation of the miracidium to the mother sporocyst of Schistosoma margrebowiei; changes in the parasite surface and implications for interactions with snail plasma factors. Parasitology 104 (1), 41–49. https://doi.org/10.1017/S0031182000060789.

de Carvalho Augusto, R., et al., 2020. Molluscicidal and parasiticidal activities of Eryngium triquetrum essential oil on *Schistosoma mansoni* and its intermediate snail host Biomphalaria glabrata, a double impact. Parasit. Vectors 13, 486. https://doi. org/10.1186/s13071-020-04367-w.

Dinguirard, N., Heinemann, C., Yoshino, T.P., 2018. Mass isolation and *in vitro* cultivation of intramolluscan stages of the human blood fluke *Schistosoma mansoni*. JoVE (J. Vis. Exp.) (131), e56345. https://doi.org/10.3791/56345.

Dunn, T.S., Yoshino, T.P., 1988. *Schistosoma mansoni*: origin and expression of a tegumental surface antigen on the miracidium and primary sporocyst. Exp. Parasitol. 67 (2), 167–181. https://doi.org/10.1016/0014-4894(88)90064-1.

Eklu-Natey, D.T., et al., 1985. Comparative scanning electron microscope (SEM) study of miracidia of four human schistosome species. Int. J. Parasitol. 15 (1), 33–42. https:// doi.org/10.1016/0020-7519(85)90098-0.

Fournier, A., Th´eron, A., 1985. Sectorisation morpho-anatomique et fonctionnelle du sporocyste-fils de*Schistosoma mansoni*. Zeitschrift für Parasitenkunde 71 (3), 325–336. https://doi.org/10.1007/BF00928335.

Fuss, A., Mazigo, H.D., Mueller, A., 2020. Malacological survey to identify transmission sites for intestinal schistosomiasis on Ijinga Island, Mwanza, north-western Tanzania. Acta Trop. 203, 105289 https://doi.org/10.1016/j. actatropica.2019.105289.

Galinier, R., et al., 2017. A multistrain approach to studying the mechanisms underlying compatibility in the interaction between Biomphalaria glabrata and *Schistosoma mansoni*. PLoS Negl. Trop. Dis. 11 (3) https://doi.org/10.1371/journal. pntd.0005398.

Guillou, F., et al., 2007. Excretory–secretory proteome of larval *Schistosoma mansoni* and *Echinostoma caproni*, two parasites of Biomphalaria glabrata. Mol. Biochem. Parasitol. 155 (1), 45–56. https://doi.org/10.1016/j.molbiopara.2007.05.009.

Hambrook, J.R., et al., 2018. A metalloprotease produced by larval *Schistosoma mansoni* facilitates infection establishment and maintenance in the snail host by interfering with immune cell function. PLoS Pathog. 14 (10), e1007393 https://doi.org/ 10.1371/journal.ppat.1007393.

Hambrook, J.R., Hanington, P.C., 2021. Immune evasion strategies of schistosomes. Front. Immunol. 11, 3820. https://doi.org/10.3389/fimmu.2020.624178.

Hansen, E., Perez-Mendez, G., 1972. Scanning electron microscopy of *Schistosoma mansoni* daughter sporocysts. Int. J. Parasitol. 2 (1), 174–IN24. https://doi.org/ 10.1016/0020-7519(72)90045-8.

Ivanchenko, M.G., et al., 1999. Continuous *in vitro* propagation and differentiation of cultures of the intramolluscan stages of the human parasite *Schistosoma mansoni*. Proc. Natl. Acad. Sci. USA 96 (9), 4965–4970.

Jourdane, J., Mingyi, X., 1987. The primary sporocyst stage in the life cycle of *Schistosoma japonicum* (Trematoda: digenea). Trans. Am. Microsc. Soc. 106 (4), 364–372. https://doi.org/10.2307/3226228.

Kamel, R.O.A., Bayaumy, F.E.-Z.A., 2017. Ultrastructural alterations in *Schistosoma mansoni* juvenile and adult male worms after *in vitro* incubation with primaquine. Memorias do Instituto Oswaldo Cruz 112, 247–254. https://doi.org/10.1590/0074- 02760160324.

Kebede, T., et al., 2020. Genetic evidence for the role of non-human primates as reservoir hosts for human schistosomiasis. PLoS Negl. Trop. Dis. 14 (9), e0008538 https://doi.org/10.1371/journal.pntd.0008538.

Kinoti, G.K., 1971. The attachment and penetration apparatus of the miracidium of schistosoma. J. Helminthol. 45 (2–3), 229–235. https://doi.org/10.1017/ S0022149X00007112.

Koie, M., Frandsen, F., 1976. Stereoscan observations of the miracidium and early sporocyst of *Schistosoma mansoni*. Z. Parasitenkd. 50 (3), 335–344. https://doi.org/ 10.1007/BF02462978.

Kruger, F.J., Hamilton-Attwell, V.L., 1988. Scanning electron microscope studies of miracidia suggest introgressive hybridization between Schistosoma haematobium and S. haematobium x S. mattheei in the Eastern Transvaal. J. Helminthol. 62 (2), 141–147. https://doi.org/10.1017/S0022149X0001138X.

Li, H., et al., 2020. Coordination of humoral immune factors dictates compatibility between *Schistosoma mansoni* and Biomphalaria glabrata. Elife 9. https://doi.org/ 10.7554/eLife.51708.

Li, S., et al., 2022. Characterization of microRNA cargo of extracellular vesicles isolated from the plasma of *Schistosoma japonicum*-infected mice. Front. Cell. Infect. Microbiol. 12:803242. doi:10.3389/fcimb.2022.803242.

Lodes, M.J., Yoshino, T.P., 1989. Characterization of excretory-secretory proteins synthesized *in vitro* by *Schistosoma mansoni* primary sporocysts. J. Parasitol. 75 (6), 853–862. https://doi.org/10.2307/3282863.

LoVerde, P.T., 1975. Scanning electron microscope observations on the miracidium of Schistosoma. Int. J. Parasitol. 5 (1), 95–97. https://doi.org/10.1016/0020-7519(75) 90104-6.

Meningher, T., et al., 2020. Schistosomal extracellular vesicle-enclosed miRNAs modulate host T helper cell differentiation. EMBO Rep. 21 (1), e47882. https://doi. org/10.15252/embr.201947882.

Meuleman, E.A., et al., 1978. Ultrastructural changes in the body wall of *Schistosoma mansoni* during the transformation of the miracidium into the mother sporocyst in the snail host Biomphalaria pfeifferi. Z. Parasitenkd. 56 (3), 227–242. https://doi. org/10.1007/BF00931716.

Pan, S.C., 1980. The fine structure of the miracidium of *Schistosoma mansoni*. J. Invertebr. Pathol. 36 (3), 307–372. https://doi.org/10.1016/0022-2011(80)90040-3.

Pereira, A.S.A., et al., 2013. Morphological and morphometric study of cercariae and adult worms of *Schistosoma mansoni* (SLM strain) isolated from infected mice. Parasitol. Res. 112 (3), 1087–1096. https://doi.org/10.1007/s00436-012-3235-9.

Portet, A., et al., 2017. Integrated multi-omic analyses in Biomphalaria-Schistosoma dialogue reveal the immunobiological significance of FREP-SmPoMuc interaction. Dev. Comp. Immunol. 75, 16–27. https://doi.org/10.1016/j.dci.2017.02.025.

Sakamoto, K., Ishii, Y., 1978. Scanning electron microscope observations on miracidium, cercaria, and cercarial papillar patterns of *Schistosoma japonicum*. J. Parasitol. 64 (1), 59–68. https://doi.org/10.2307/3279610.

Samuelson, J.C., Caulfield, J.P., 1985. Role of pleated septate junctions in the epithelium of miracidia of *Schistosoma mansoni* during transformation to sporocysts *in vitro*. Tissue Cell 17 (5), 667–682. https://doi.org/10.1016/0040-8166(85)90003-5.

Yoshino, T.P., Gourbal, B., Theron, A., 2016, 2016. In: Jamieson, B.G.M. (Ed.), Schistosoma: biology, pathology and control, 31. CRC Press, pp. 978–1498744256.

Yoshino, T.P., Laursen, J.R., 1995. Production of *Schistosoma mansoni* daughter sporocysts from mother sporocysts maintained in synxenic culture with biomphalaria glabrata embryonic (BGE) Cells. J. Parasitol. 81 (5), 714–722. https:// doi.org/10.2307/3283960.

Yoshino, T.P., Lodes, M.J., 1988. Secretory protein biosynthesis in snail hemocytes: *in vitro* modulation by larval schistosome excretory-secretory products. J. Parasitol. 74 (4), 538–547. https://doi.org/10.2307/3282169.

Zoghroban, H.S., et al., 2019. Niosomes for enhanced activity of praziquantel against *Schistosoma mansoni: in vivo* and *in vitro* evaluation. Parasitol. Res. 118 (1), 219–234. https://doi.org/10.1007/s00436-018-6132-z.